Exocytosis coordinates epithelial cell-turnover in *Drosophila* ribosomal protein mutants

Nanami Akai[1], Tatsushi Igaki[2], and Shizue Ohsawa[1, *]

[1]*Group of Genetics, Division of Biological Science, Graduate School of Science, Nagoya University, Furo-cho, Chikusa-ku, Nagoya, Aichi, 464-8602, Japan*

[2]*Laboratory of Genetics, Graduate School of Biostudies, Kyoto University, Yoshida-Konoe-cho, Sakyo-ku, Kyoto 606-8501, Japan.*

[*] To whom correspondence should be addressed:
Shizue Ohsawa, Ph.D.
E-mail: ohsawa.shizue.x5@f.mail.nagoya-u.ac.jp
TEL: +81-52-789-2994
FAX: +81-89-789-2995

Running Title: Exocytosis drives epithelial cell-turnover

Abstract

Robust tissue growth is orchestrated by the precise coordination of cell death and cell proliferation. Our previous study found that in the developing wing pouches of *Drosophila Minute*/+ animals, both cell death and compensatory cell proliferation are dramatically increased, which contributes to robust growth of mutant tissue. The induction of this cell-turnover depends on activation of JNK signaling, although the mechanism by which JNK activation causes cell-turnover remained unclear. Here, we found that JNK-mediated elevation of exocytosis in dying cells is crucial for inducing cell-turnover in *M/*+ wing morphogenesis. Mechanistically, elevated JNK signaling in dying cells upregulates exocytosis-related genes and Wingless (Wg), leading to enhanced Wg secretion. Our data also suggested that secreted Wg from dying cells enhances Wg signaling activity in neighboring living cells via their Frizzled-2 (Fz2) receptors. This interaction between dying cells and their neighboring living cells is pivotal in determining cell fate, dictating which cells will undergo apoptosis and which cells will proliferate. Our findings provide mechanistic insights into the complex interplay between cell death and proliferation, governed by exocytosis and Wg signaling, in coordinating robust tissue growth.

Introduction

Ribosomes are essential molecular machines responsible for protein synthesis in living cells, and thus fundamental to life. In humans, heterozygosity of genes related to ribosomal proteins or ribosomal biogenesis factors leads to a group of genetic disorders collectively termed ribosomopathies. For instance, heterozygous mutations in various ribosomal protein genes, including *RPS17* (1), *RPS26* (2), *RPS19* (3), *RPS24* (4), and *RPL27* (5), are associated with Blackfan anaemia (DBA), with some patients exhibiting tissue-specific developmental anomalies such as limb defects, cleft palate, and abnormal heart development (6, 7). In addition, heterozygous mutations in the *RpSA* gene are linked to isolated congenital asplenia (ICA), a disorder characterized by the absence of a spleen at birth (8). However, the precise mechanisms by which a reduction in ribosomal protein gene dosage leads to these genetic disorders remain elusive.

In *Drosophila*, a series of heterozygous mutants for ribosomal protein genes, called *Minute/+* (*M/+*), exhibit a pronounced developmental delay during larval stages (9). Despite this significant delay, *M/+* animals are essentially normal flies without noticeable morphological defects, except for the thinner bristles, suggesting that *M/+* animals exert certain mechanisms to overcome developmental perturbations caused by reduced ribosomal protein levels. It has been reported that extensive cell death (10), as well as cellular stress (10, 11, 12, 13), is a distinctive characteristic of the *M/+* wing pouch. Our previous study (14) has shown that apoptotic cell death and the subsequent cell proliferation are dramatically increased in the *M/+* wing pouch. Blocking this cell-turnover by inhibiting cell death resulted in morphological abnormalities, indicating the essential role of cell-turnover in *M/+* wing morphogenesis. Genetic analyses have revealed that the induction of this cell-turnover depends on activation of JNK signaling. However, downstream events of JNK activation remain to be elucidated.

The coordination of cell death and proliferation through cell-cell communications is crucial for proper development and homeostasis of multicellular organisms. Apoptotic cells, for example, can secrete mitogens such as Winless (Wg; a Wnt homolog), dpp (a BMP homolog), and Hh, which could promote the proliferation of nearby cells in the *Drosophila* epithelium (15, 16, 17, 18). Cell competition, a phenomenon in which cells with higher fitness ("winners") eliminate neighboring less fit cells ("losers") by

75 inducing cell death (19), is another aspect of cell-turnover. It has been reported that
76 secretory factors from prospective loser cells contribute to cell competition. For
77 instance, the cytokine-like ligand unpaired 3 (upd3) produced by losers promotes cell
78 competition between wild-type (winners) and *M/+* cells (losers) in the *Drosophila*
79 epithelium (12). Furthermore, Madin-Darby canine kidney cells depleted of the polarity
80 regulator gene *scribble* (*scrib*^{KD} MDCK cells) secrete Fibroblast Growth Factor 21
81 (FGF21), which in turn promotes cell competition with neighboring wild-type MDCK
82 cells (20). However, the mechanism by which these secreted factors from dying cells
83 orchestrate both their own cell death and the proliferation of neighboring living cells is
84 still not fully understood.

85 Here, we found that exocytosis, as a downstream event of JNK signaling in dying
86 cells, contributes to cell-turnover in the *M/+* wing pouch, which is essential for robust
87 wing development in *M/+* animals. Our genetic analyses suggest that elevated
88 exocytosis likely facilitates the release of Wg from dying cells, which in turn stimulates
89 their own cell death and the proliferation of neighboring living cells. Our observations
90 could provide new mechanistic insights into how dying cells coordinate robust
91 development through cell-cell interactions.

92

93

94 Results

95 *M/+* wing pouch elevates exocytosis downstream of JNK signaling

96 To elucidate the downstream event of JNK signaling in the *M/+* wing pouch, we
97 conducted RNA sequence (RNA-seq) analyses on GFP-labeled fluorescence-activated
98 cell sorting (FACS)-sorted wing pouch cells from one of the *M/+* mutants *RpS3/+*,
99 compared to GFP-labeled wild-type control or *RpS3/+* wing pouch cells overexpressing
100 JNK inhibitor Puckered (Puc) (Fig S1A; the wing pouch is green-marked oval domain
101 that becomes the adult wing blade). Among the 1,097 genes that were upregulated or
102 downregulated in the *RpS3/+* wing pouch relative to the wild-type, we identified
103 positive regulators of JNK signaling such as *reaper* and *pvf1*, JAK/STAT targets
104 including *Socs36E* and c*hinmo*, Gr64 gustatory receptors and numerous genes
105 associated with oxidative stress and DNA repair (Fig S1B, S1 Table, and S3 table),
106 which aligns with previous reports on genes upregulated in the *RpS3/+* or *RpS17/+*

107 wing disc (12, 13). These data validate our experimental conditions for identifying
108 genes required for JNK-mediated events in the *M/+* wing pouch.

109 Mining the list of genes differentially expressed in the *RpS3/+* wing pouch cells
110 dependent on JNK signaling (Fig S1C and S2 Table), we noticed that among the genes
111 associated with the "secretion by cell" GO term (Fig S1B), the evolutionarily conserved
112 exocytosis-related genes *unc-13*, *SNAP25,* and *cadps* (*Calcium-dependent secretion*
113 *activator*) were upregulated in a JNK-dependent manner (Fig S1D). Among these
114 exocytosis-related genes, the upregulation of *SNAP25* and *unc-13* was consistent with
115 the previous reports concerning genes upregulated in *RpS3/+* or *RpS17/+* cells (12, 13) .

116 Calcium-dependent exocytosis is the process whereby cells release intracellular
117 contents into the extracellular space. It has been shown that *unc-13, SNAP25*, and *cadps*
118 collectively regulate the docking process of secretory vesicles to the plasma membrane
119 during Ca^{2+}-mediated exocytosis ((21, 22, 23), Reviewed in (24)). First, to investigate
120 whether exocytosis is upregulated in the *M/+* wing pouch, we utilized the exosome
121 marker CD63 tagged with EGFP (EGFP-CD63) (25, 26, 27, 28). Additionally, we
122 utilized Syt1 tagged with EGFP (Syt1-EGFP), a widely used vesicle marker prevalent
123 in both neuronal and non-neuronal cells (29, 30, 31). We observed a significant increase
124 in EGFP-CD63- positive and Syt1-EGFP-positive vesicles in the *RpS3/+* wing pouch
125 compared to the wild-type control (Fig 1A, 1B, 1G and 1H, corresponding to the boxed
126 region in Fig 1E, quantified in Fig 1F and Fig 1K). EGFP-CD63-positive vesicles were
127 also found to be increased in the *RpL19/+* wing pouch (Fig S1E, quantified in Fig S1F).
128 Notably, these vesicles were predominantly observed in regions of the *RpS3/+* wing
129 pouch undergoing massive cell death (as indicated by arrowheads in Fig 1B, 1H, and
130 S1E), a phenomenon we previously reported (14) and also confirmed in this study
131 (shown in Fig 2G, compared to Fig 2F, quantified in Fig 2Q). Furthermore, we noted
132 an increase in vesicles positive for the ESCRT protein Hrs, another exosome marker,
133 in the *RpS3/+* wing pouch relative to the wild-type control (Fig S1G and S1H,
134 quantified in Fig S1I). To further investigate the enhanced exocytosis in the *RpS3/+*
135 wing pouch, we utilized the GCaMP6m fluorescent calcium reporter (32) to monitor
136 Ca2+ activity, a known inducer of exocytosis. We observed persistent Ca^{2+} activity in
137 morphologically dying cells, along with spontaneous Ca^{2+} flashes similar to those in
138 the wild-type control (Fig 1L and 1M, quantified in Fig 1P). This persistent activity
139 suggested an enhanced exocytic process in dying cells in the *M/+* wing pouch,
140 potentially driven by elevated calcium levels.

141 We then examined whether exocytosis is the downstream event of JNK activation
142 in the *M/+* wing pouch. We found that blocking JNK signaling by overexpressing Puc
143 significantly suppressed the increased number of EGFP-CD63/Syt1-EGFP-positive
144 vesicles, as well as the emergence of cells exhibiting persistent Ca^{2+} signaling (Fig 1C,
145 quantified in Fig 1F; Fig 1I, quantified in Fig 1K; Fig 1N, quantified in Fig 1P).
146 Together, these observations suggest that exocytosis is elevated in dying cells within
147 the *M/+* wing pouch as a downstream event of JNK signaling.
148
149 **Exocytosis is required for massive cell-turnover in the *M/+* wing pouch**
150 We have previously demonstrated that JNK signaling is required for cell-turnover
151 in the *M/+* wing pouch (14). In line with our previous study, using the *puc-gal4* driver,
152 where *gal4* is driven by the JNK target gene *puc* promoter, we observed JNK activation
153 in the *RpS3/+* wing pouch compared to the wild-type control (Fig 2M and 2N).
154 Blocking JNK signaling by overexpressing Puc significantly reduced cell death and
155 mitoses in the *RpS3*/+ wing pouch, as assayed by the CD8-PARP-Venus probe for
156 caspase activity in the imaginal disc (33, 34, 35, 36, 37, 38, 39, 40), and the M phase
157 marker phospho-Histone H3 (Fig 2A-2C, quantified in Fig 2P; Fig 2F, 2G and S2A,
158 quantified in Fig S2N). In addition, we intriguingly found that downregulating *unc-13*,
159 a docking factor involved in exocytosis, similarly diminished cell death and mitoses
160 (Fig 2H and S2B, quantified in Fig 2Q and S2N, respectively; Fig 2D, quantified in Fig
161 2P), and also reduced EGFP-CD63-positive and Syt1-EGFP-positive vesicles in the
162 *RpS3*/+ wing pouch (Fig 1D and 1J, quantified in Fig 1F and 1K, respectively).
163 Knocking down *rab3*, a "Secretory GTPase Rabs" required for vesicle exocytosis, also
164 significantly reduced cell death and mitoses in the *RpS3*/+ wing pouch (Fig 2I and S2C,
165 quantified in Fig 2Q and S2N, respectively; Fig 2E, quantified in Fig 2P). Furthermore,
166 overexpressing Puc or downregulating either *unc-13* or *rab3* led to morphological
167 defects in the *RpS3/+* adult wing, while their individual overexpression or
168 downregulation did not affect wing development (Fig 2K, 2L, and S2K). These results
169 suggest that exocytosis, as a downstream component of JNK signaling, is pivotal for
170 cell turnover and subsequent normal morphogenesis in the *M/+* wing pouch. Indeed,
171 downregulating other docking factors such as *SNAP25* or *Syt1* (41), another Secretory
172 GTPase *Rab27*, or *ALIX*, an ESCRT (endosomal sorting complexes required for
173 transport)-related protein involved in the biogenesis of extracellular vesicles (42, 43),
174 also significantly suppressed cell death in the *RpS3*/+ wing pouch (Fig 2J, quantified in

175 Fig 2Q; Fig S2D-S2J, quantified in Fig S2N). In addition, using the *puc-gal4* driver,
176 *Rab3* knockdown in JNK-activating cells notably reduced cell death in both *RpS3/+*
177 and *RpL19/+* wing discs (Fig 2N and 2O, quantified in Figs 2R; Fig S2L and S2M,
178 quantified in Fig S2O). Together, these data reinforce the vital role of exocytosis in cell
179 turnover within the M/+ wing pouch, functioning as a downstream process of JNK
180 signaling.
181
182 **Dying cells secrete Wg via exocytosis in the *M/+* wing pouch**
183 We next aimed to identify the protein secreted through exocytosis from dying cells
184 in the *M/+* wing pouch. Our previous genetic analyses (14) indicated that cell-turnover
185 in the *M/+* wing pouch is initiated by a mechanism akin to Wg-dependent cell
186 competition, a phenomenon by which cells with higher Wg signaling activity eliminate
187 neighboring cells with lower Wg signaling activity in the wing disc (44). Indeed, areas
188 exhibiting massive cell death corresponded to regions showing relatively lower Wg
189 signaling activity, as indicated by the *nmo-lacZ* reporter (Fig S3A), a finding also
190 reported in our previous study (14). In addition, we have previously shown that
191 genetically reducing the Wg signaling gradient in the entire *M/+* pouch significantly
192 suppressed cell death (14). These our observations prompted us to consider the idea that
193 dying cells in the *M/+* wing pouch might release Wg via JNK-mediated exocytosis,
194 potentially conferring a survival advantage to their neighboring living cells. Consistent
195 with this hypothesis, it has been reported that Wnt/Wg can be released through
196 extracellular vesicles including exosome (26, 45, 46, 47, 48). Interestingly, we found
197 that the *RpS3/+* wing pouch expressing the cell death inhibitor p35 (which allows dying
198 *RpS3/+* cells to survive) exhibited elevated levels of Wg protein, compared to the wild-
199 type control (Fig 3A and 3B). This increase in Wg protein was significantly diminished
200 by overexpressing the JNK inhibitor Puc (Fig 3C), suggesting that Wg expression is
201 upregulated via JNK signaling in the *M/+* wing pouch, similar to apoptotic cells in
202 which JNK signaling induces the production of secreted growth factor, including Wg
203 (17, 49, 50). In addition, we noted that GFP-Wg-positive puncta, derived from a knock-
204 in allele (51), were increased in the area with massive cell death in the *RpS3/+* wing
205 pouch, compared to the wild-type control (Fig 3D and 3E). This increase in GFP-Wg-
206 positive puncta was more evident when using a membrane-tethered anti-GFP nanobody
207 (Vhh4-CD8), which immobilizes GFP-Wg on the cell surface (51) (Fig 3G and 3H,
208 quantified in Fig 3K). Intriguingly, these GFP-Wg-positive puncta sometimes

209 colocalized with CD63-mCherry-positive vesicles (Fig 3E and Fig S3C, indicated by
210 arrowheads), suggesting the possibility that GFP-Wg might be secreted via
211 extracellular vesicles through JNK-mediated exocytosis. To support this possibility, we
212 found that blocking JNK signaling by overexpressing Puc or knocking down *unc-13*
213 significantly reduced the number of GFP-Wg-positive puncta in the *RpS3/+* wing
214 pouch (Fig 3I and 3J, quantified in Fig 3K). In addition, we observed a significant
215 increase in extracellular GFP-positive puncta and extracellular CD63-mCherry-positive
216 vesicles in the *RpS3/+* wing pouch when GFP-Wg was captured using the Vhh4-CD8
217 morphotrap on the cell surface, compared to the wild-type control (Fig S3D and S3E,
218 quantified in Fig S3F and Fig S3G). Furthermore, these extracellular GFP-positive
219 puncta captured on the cell surface by the Vhh4-CD8 morphotrap occasionally
220 colocalized with extracellular CD63-mCherry-positive vesicles (6.88% in the wild-type,
221 and 16.45% in the *RpS3/+* wing pouch region, which is characterized by massive cell
222 death, as indicated by the arrowheads in Fig S3D and S3E). Together, these data suggest
223 that dying cells secrete Wg via exocytosis in the *M/+* wing pouch.
224
225 **Fz2 contributes to massive cell-turnover in the *M/+* wing pouch**
226 Finally, we investigated the potential role of the Wg receptor in mediating cell-
227 turnover in the *M/+* wing pouch, which could interact with Wg released from dying
228 cells. We found that the expression of the Wg receptor Frizzled2 (Fz2) (52, 53, 54) was
229 upregulated in the *RpS3/+* wing pouch compared to the wild-type control, as assayed
230 by the *Fz2-lacZ* (55) and the *Fz2-Venus* protein trap (56, 57) (Fig 4A-4C, quantified in
231 Fig 4F; Fig S4A-S4C). Additionally, a downregulation of Fz2 expression was observed
232 in the dying cells of the *M/+* wing pouch (Fig 4B, 4C, S4B and S4C), which is
233 associated with JNK signaling (Fig 4D and S4D), though it is unclear whether this is
234 directly mediated by JNK signaling or a consequence of JNK-mediated dying process.
235 Furthermore, we intriguingly found that cell death and mitoses were significantly
236 suppressed in the *M/+* wing pouch when the difference in Fz2 expression level was
237 reduced, either by deleting one copy of the Fz2 gene or by knocking down *Fz2*
238 throughout the entire wing pouch (Fig 4G-4I and 4K, quantified in Fig 4J and 4L,
239 respectively). These observations are consistent with our previous study, which
240 demonstrated that cell death was significantly suppressed when the Wg signaling
241 gradient in the *M/+* pouch was genetically reduced (14). Taken together, these results
242 suggested that the elevated expression of Fz2 in the M/+ wing pouch, relative to the

243 wild-type control, plays a critical role in potentially facilitating the activation of Wg
244 signaling in response to Wg released from dying cells, thereby driving massive cell
245 turnover in the M/+ pouch.
246
247
248 **Discussion**
249 Our current study reveals that exocytosis is crucial for massive cell-turnover in
250 *M/+* wing morphogenesis, functioning as a downstream event of JNK signaling. In
251 dying cells, JNK signaling elevates the expression of exocytosis-related genes and Wg,
252 leading to increased Wg secretion. This secreted Wg likely interacts with the Fz2
253 receptors on neighboring living cells, enhancing Wg signaling and thereby determining
254 their cell fates by specifying which cell undergo apoptosis and which are primed for
255 proliferation (Fig. 5). Notably, impairment of exocytosis in dying cells in *RpS3/+*
256 animals leads to phenotypic variations in adult wings (Fig 2K and 2L in this study),
257 suggesting that increased exocytosis in dying cells, followed by subsequent cell-
258 turnover, may provide the flexibility needed to adjust developmental programs.
259 We identified Wg as a crucial factor secreted through exocytosis from dying cells,
260 which is essential for the proliferation of neighboring living cells to maintain tissue
261 homeostasis. Previous studies have shown that 'undead' cells, stimulated toward
262 apoptosis but kept alive by the caspase inhibitor p35, are able to promote the
263 proliferation of neighboring cells in the *Drosophila* epithelium (58, 59, 60). Several
264 mitogens including Wg, Dpp, and Spitz (a EGF homolog) have been identified as being
265 produced by apoptotic cells in a JNK-dependent manner (17, 50, 61). In addition,
266 Hedgehog (Hh) (15) have also been identified as products of apoptotic cells.
267 Furthermore, during cell competition between wild-type (winners) and *M/+* cells
268 (losers) in the *Drosophila* epithelium, prospective loser cells secrete Upd3, which
269 promotes competitive elimination by winner cells (12). Hence, in addition to Wg, other
270 mitogens could also be secreted thorough exocytosis from dying cells, potentially
271 contributing to massive cell-turnover in the *M/+* wing pouch.
272 Previous studies have identified exosomes as carriers of Wnt/Wg in the
273 extracellular space of both mammalian and *Drosophila* cells, including wing disc cells
274 (26, 45, 46, 47, 48, 62). Concurrently, alternative mechanisms for Wg transport, such
275 as those involving lipoprotein particles or a lipocalin Swim in the *Drosophila* wing disc,
276 have been reported (27, 63). Additionally, the cell-surface proteoglycan Dally-like-

277 protein (Dlp) has been reported to enable long-range signaling of the palmitoylated Wg
278 (51). Our data from the *M/+* wing disc reveal partial colocalization of Wg-GFP puncta
279 with exosome markers such as CD63-mCherry and Hrs. This indicates that while
280 exosomes contribute significantly to Wg transport, other mechanisms may also be
281 involved. Importantly, our study stands out by focusing on Wg transport in the unique
282 context of the *M/+* wing pouch, which is characterized by massive cell turnover
283 essential for normal development. This suggests the potential for Wg transport
284 mechanisms to be highly context-dependent, particularly in environments with active
285 cellular dynamics.

286 *Rp* genes are crucial in a broad range of organisms, from yeast to humans,
287 frequently exhibiting haploinsufficient mutant phenotypes. Notably, heterozygous
288 mutations in genes encoding ribosomal proteins or ribosomal biogenesis factors are
289 linked to tissue-specific human diseases known as ribosomopathies (64). In patients
290 affected by these conditions, some tissues may preserve normal patterning and
291 functions, potentially by buffering stresses caused by ribosomal mutations. Given the
292 evolutionary conservation of the molecules we identified in *Drosophila*, regulating cell
293 turnover through exocytosis in dying cells may represent evolutionarily conserved
294 strategy to prevent developmental abnormalities in ribosomal protein mutants.
295
296

297 # Method

298

299 **Fly strains**

300 Fly stocks were cultured at 25°C on standard fly food. To detect dying cells in the wing
301 pouch, the following strains were used: *nub-Gal4; UAS-CD8-PARP-Venus* (control);
302 *nub-Gal4; UAS-CD8-PARP-Venus, RpS3^{Plac92}/TM6B* (*RpS3*/+ tester); *puc-Gal4, UAS-*
303 *CD8-PARP-Venus/TM6B.* Additional strains were used as follows: *UAS-*
304 *EGFP.CD63* (BL91390), *UAS-CD63.mCherry* (BL91389), *UAS-Syt1-eGFP* (BL6925),
305 *RpL19^{K03704}* (DGRC102285), *20XUAS-IVS-GCaMP6m* (BL42750), *UAS-unc-13-RNAi*
306 (VDRC33609, NIG2999R-2), *UAS-LexA-RNAi* (BL67947), *UAS-Rab3-RNAi*
307 (NIG7576R-3, BL31691), *UAS-SNAP25-RNAi* (HMS01367, BL27306), *UAS-Syt1-*
308 *RNAi* (NIG3139R-1, BL31668), *UAS-Rab27-RNAi* (NIG14791R-2, BL31887), *UAS-*
309 *ALiX-RNAi* (HMS00298, VDRC32049), *UAS-fz2-RNAi* (NIG9739R-1, 9739R-2),

310 *UAS-Puc* (65), *UAS-p35* (66), *nmo*^{P1} (BL27897), *fz2*^{CPTI003490} (*fz2-Venus*)
311 (DGRC115411), *fz2*^{SB227} (*fz2-lacZ*) (DGRC103079), *GFP-Wingless*^{S239A} (JP. Vincent)
312 (51), *UAS-VHH4-CD8-HA* (JP. Vincent) (51), and *fz2*^{C1} (G. Struhl) (67).
313
314 **Histology**
315 Wandering third instar larvae were dissected in phosphate buffered saline (PBS) and
316 fixed with 4%-Paraformaldehyde (PFA) for 5 min on ice, followed by 20 min at room
317 temperature. The fixed larvae were washed 3 times with PBT (PBS + 0.1% TritonX100)
318 for 20 min each, and were then blocked with PBTn (5% donkey serum + PBT) solution
319 for 30 min. For immunostaining, they were incubated overnight at 4°C with primary
320 antibodies in PBTn. After four 30-minute washes with PBT, the samples were re-
321 blocked in PBTn for 30 minutes, then incubated with secondary antibodies for 2 hours
322 at room temperature. Following another set of four 30-minute washes with PBT, the
323 samples were mounted using either SlowFade Diamond Antifade Mountant (Invitrogen,
324 #S36972) or an alternative anti-fade mounting medium. The latter was composed of
325 70% Glycerol (Sigma, #G5516), 0.2% n-Propyl Gallate (KANTO CHEMICAL,
326 #32465-31), and supplemented with DAPI (Sigma, #D9542). For extracellular
327 immunostaining, larvae were dissected in ice-cold Schneider's *Drosophila* Medium
328 (Gibco, #21720024) and incubated with primary antibodies for 2 hours on ice. The
329 larvae were then rinsed with ice-cold Schneider's *Drosophila* Medium followed by
330 PBS and fixed with 4% PFA for 40 min at room temperature. After fixation, samples
331 were washed with PBS. Subsequent processing was the same as in the preceding
332 protocol. Images were taken with Leica SP5, Leica SP8, Leica SPE, Leica STELLARIS
333 and ZEISS LSM900 confocal microscopes. Primary antibodies used are as follows; rat
334 anti-GFP antibody (Nacalai Tesque, #04404-26, 1:1000) (Extracellular GFP, 1:300),
335 rabbit anti-cleaved PARP (Asp214) antibody (Cell Signaling Technology (CST), #9541,
336 1:200), rabbit anti-phospho-histone H3 (Ser10) antibody (CST, #9706, 1:100), mouse
337 anti-Wg antibody (Developmental Studies Hybridoma Bank (DSHB), #4D4-c, 1:500),
338 rabbit anti-DsRed antibody (Takara Bio Clontech (CLN), #632496, 1:250)
339 (Extracellular DsRed, 1:75), mouse anti-β-galactosidase antibody (Sigma, #G8021,
340 1:500), mouse anti-Hrs antibody (DSHB, #27-4-s, 1:250), and rabbit anti-Cleaved
341 *Drosophila* Dcp-1 (Asp216) antibody (CST, #9678, 1:100) for 3 days. Secondary
342 antibodies used are as follows; Goat anti-rabbit Alexa 488 (1:250, Invitrogen #A11034),

343 Goat anti-rabbit Alexa 546 (1:250, Invitrogen #A11035), Goat anti-rat Alexa 488
344 (1:250, Invitrogen #A11006), Goat anti-chicken Alexa 488 (1:250, Invitrogen,
345 #A11039), and Goat anti-mouse Alexa 647 (1:250, Invitrogen #A21237) antibodies.
346
347 **Quantification of puncta number**
348 The vesicle marker EGFP-CD63, CD63-mCherry, and Syt1-eGFP were expressed in
349 the wing pouch under the control of *nub-gal4 driver*. In the region where massive cell
350 death is observed in the *M/+* wing disc, these markers, in addition to GFP-Wingless
351 signals, were acquired at the confocal plane exhibiting the highest signal intensity.
352 Puncta were manually counted using Fiji software and the data were analyzed with
353 KaleidaGraph (Synergy Software).
354
355 **Calcium Time-lapse imaging and quantification**
356 To monitor Ca^{2+} activity, wandering third instar larvae were dissected and cultured in
357 Schneider's *Drosophila* medium supplemented with 2% FBS, 1% Insulin solution
358 (Sigma-Aldrich, #I0516), 3% fly extract (VDRC, #VFE1.25), and 2% low-melting
359 agarose (Sigma-Aldrich, #A4018)/PBS. Imaging was conducted at 10 sec intervals for
360 20-min with a Leica STELLARIS confocal microscope (38, 68). For quantitative
361 analysis, dying cells exhibiting continuous calcium activity were manually counted
362 using Fiji software and the data were analyzed with KaleidaGraph.
363
364 **Detection of dying cells and quantification using CD8-PARP-Venus**
365 To detect dying cells, the activated-caspase-3 indicator CD8-PARP-Venus was
366 expressed in the pouch under the control of *nub-gal4* driver or JNK activating cells
367 under the control of *puc-gal4* driver. Cleaved PARP signals were acquired at the
368 confocal plane where signal intensity was highest. The number of these signals in the
369 wing pouch was manually measured using Fiji software and the data were analyzed
370 with KaleidaGraph.
371
372 **Quantification of pH3-positive area**
373 For the analysis of pH3-positive cells, total area of pH3-positive cells and the size of
374 the wing pouch area were automatically measured from confocal slices of Z-stack
375 images compressed using maximum projection functions in Fiji software, as previously
376 described (69). The acquired data were then analyzed with KaleidaGraph.

377

378 **Measurement of adult wings**

379 Left and right wings of female flies were rinsed with xylene and mounted in a Canada
380 Balsam (Nacalai Tesque). Images of the wings were acquired using Leica M205C
381 stereo microscope.

382

383 **Quantitative Analysis of GFP-Wingless and CD63-mCherry Colocalization**

384 To analyze the overlap between GFP-Wingless-positive puncta and CD63-mcherry-
385 positive vesicles, their colocalization was manually quantified in the regions exhibiting
386 massive cell death. This quantification was conducted using the confocal plane that
387 displayed the highest signal intensity. Images were manually thresholded to eliminate
388 background signals, and the areas of overlap were calculated using Fiji software,
389 followed by further analyses with KaleidaGraph.

390

391 **Quantification of *Fz2-lacZ* signals**

392 For comparing *Fz2-lacZ* expression levels, single confocal sections were used, and a
393 fluorescence intensity profile was generated by measuring the fluorescence intensity of
394 *Fz2-lacZ*-expressing cells along the dorsal compartment (the pale yellow-marked area
395 indicated in Fig 4E) using Fiji software.

396

397 **FACS and mRNA-seq analysis**

398 GFP+ wing pouch cells were isolated using a FACS Aria II cell sorter (BD Bioscience).
399 Total RNA was then extracted for RNA sequencing analysis, following the method
400 previously described (70). Briefly, third instar larvae were dissected in ice-cold PBS.
401 The wing disc cells were dissociated using Trypsin (10x TrypLE Select) (Gibco,
402 #A1217701) at 37ºC for 20 min. The enzymatic reaction was stopped with Schneider's
403 medium containing 5% FBS, and GFP-positive cells from wing pouches were sorted
404 using a FACS Aria II cell sorter (BD Bioscience). RNA samples were extracted using
405 NucleoSpin RNA XS Kit (TaKaRa, #740902). The quality of the extracted total RNA
406 was assessed using an Agilent 2100 Bioanalyzer, and then Strand-specific Libraries for
407 mRNA-seq were prepared using the NEBNext Ultra II Directional RNA Library Prep
408 Kit for Illumina (E7760S). For RNA-seq, NextSeq 500/550 High output Kit v2.5 was
409 utilized on a NextSeq 500 (Illumine), generating single-end reads at a length of 85 bases.

410

411 **RNA-seq data analysis**

412 Each genotype was analyzed across three independent replicates. Each sequencing
413 experiment generated more than 16 million raw reads. These reads were then quality-
414 filtered using Trim_Galore! (v0.6.5)
415 (https://www.bioinformatics.babraham.ac.uk/projects/ trim_galore/) with the default
416 setting to remove low-quality reads and adaptor sequences. The filtered reads were
417 mapped to the *Drosophila* melanogaster genome (Ensembl BDGP6.32), obtained from
418 Illumina iGenomes using STAR (71). In the *RpS3/+, nub-Gal4, UAS-Puc* experiment,
419 one sample exhibited only 65.69% of reads being uniquely mapped, which was lower
420 compared to other experiments where more than 80% of reads were uniquely mapped
421 in each sample. The number of reads mapped to each gene was quantified using RSEM
422 (v1.3.3) (72). Normalization was performed with calcNormFactors function in edgeR
423 (v3.30.3) (73). Significantly differentially expressed genes were identified with an
424 FDR<0.05 using the glmQLFit and glmQLFTest function in edgeR (R version 4.0.1,
425 limma 3.44.3). Furthermore, GO enrichment analysis was performed on the 362 genes
426 regulated by JNK signaling, utilizing the online tool available at "Gene Ontology"
427 (https://geneontology.org).

428

429 **Statistical analysis**

430 Statistical analysis was performed, and boxplot graphs were generated using
431 KaleidaGraph ver4.5 (Synergy Software). All experiments represented in the same
432 graph were conducted at the same time. In bar graphs, error bars indicate the standard
433 deviation (SD). Significance levels are indicated as follows: * P<0.05, ** P<0.01, and
434 *** P<0.001. All statistical data were summarized in S4 Table.

435

436

437 ## Author Contributions

438 **Conceptualization:** Nanami Akai, Tatsushi Igaki, Shizue Ohsawa.

439 **Data curation:** Nanami Akai, Tatsushi Igaki, Shizue Ohsawa.

440 **Formal analysis:** Nanami Akai.

441 **Funding acquisition:** Shizue Ohsawa, Tatsushi Igaki.

442 **Investigation:** Nanami Akai, Shizue Ohsawa.

443 **Methodology:** Nanami Akai.

Project administration: Shizue Ohsawa.

Resources: Shizue Ohsawa.

Supervision: Shizue Ohsawa.

Visualization: Nanami Akai, Tatsushi Igaki, Shizue Ohsawa.

Writing – original draft: Nanami Akai, Shizue Ohsawa.

Writing – review & editing: Nanami Akai, Tatsushi Igaki, Shizue Ohsawa.

Acknowledgments

We thank Takefumi Kondo, Keisuke Ikawa, Kiichiro Taniguchi, Rina Nagata, and Yukari Sando for discussions, Susumu Tsutsumi, Nana Watanabe, Mina Hoshino, Tomoko Furukawa, and Sayako Suzuki for technical support, and NGS core facility of the Graduate Schools of Biostudies, Kyoto University for supporting the RNA-seq analysis. We also thank Yash Hiromi, Gary Struhl, Maoto Sato, Jean-Paul Vincent, the Bloomington *Drosophila* Stock Center (Indiana), the Vienna *Drosophila* Resource Center (Vienna), the National Institute of Genetics Stock Center (Mishima), and the *Drosophila* Genomics and Genetic Resources (Kyoto) for fly stocks. Cell sorting using BD FACS Aria II were performed at the Medical Research Support Center, Graduate School of Medicine, Kyoto University, supported by Basis for Supporting Innovative Drug Discovery and Life Science Research (BINDS) from AMED (Grant No. JP22ama121034). This work was supported in part by MEXT Grant-in-Aid (KAKENHI) for Transformative Research Area (A) (Grant Nos. 20H05945 to SO, 21H05284 to TI), the Scientific Research (B) (Grant No. 22H02616 to SO), and Challenging Exploratory Research (Grant No. 21K19257 to SO), Japan Science and Technology Agency (Moonshot Research & Development: Grant Number JPMJPS2022 to SO), AMED-CREST, Japan Agency for Medical Research and Development (22gm1710002h0001 to TI), and Japan Agency for Medical Research and Development (21gm5010001 to TI) .

473 # Figure legends
474
475 **Fig 1. *M/+* wing pouch elevates exocytosis downstream of JNK signaling**
476 **(A-E)** The exosome marker EGFP-CD63 was expressed in the wing pouch of wild-type,
477 (A), *RpS3/+,* (B), *RpS3/+, nub-Gal4, UAS-Puc* (C), or *RpS3/+, nub-Gal4, UAS-unc-*
478 *13-RNAi* (D) flies (white). The images correspond to the boxed area in the schematic
479 diagram of the wing disc (E). Dying cells in the wing disc were visualized by anti-
480 cleaved Dcp-1 staining (white). EGFP-CD63-positive vesicles were frequently
481 observed in the area of morphological dying cells in the *RpS3/+* wing pouch (Indicated
482 by Orange arrowheads). Scale bar, 50 μm.
483 **(F)** Boxplot with dots representing the number of EGFP-CD63-positive puncta in the
484 pouch of genotypes shown in (A) (n=13, number of wing pouches), (B) (n=14), (C)
485 (n=16), and (D) (n=13). Error bars, SEM; ***, $p<0.001$; Wilcoxon rank-sum test.
486 **(G-J')** The vesicle marker Syt1-EGFP was expressed in the wing pouch of wild-type
487 (G), *RpS3/+* (H), *RpS3/+, nub-Gal4, UAS-Puc* (I), or *RpS3/+, nub-Gal4, UAS-unc-13-*
488 *RNAi* (J) flies (white). The images correspond to the boxed area in the schematic
489 diagram of the wing disc (E). Dying cells in the wing disc were visualized by anti-
490 cleaved Dcp-1 staining (white). Syt1-EGFP-positive vesicles were frequently observed
491 in the area of morphological dying cells in the *RpS3/+* wing pouch (Indicated by Orange
492 arrowheads). Scale bar, 50 μm.
493 **(K)** Boxplot with dots representing the number of Syt1-EGFP-positive puncta in the
494 wing pouch of genotypes shown in (G) (n=15), (H) (n=12), (I) (n=14), and (J) (n=16).
495 Error bars, SEM; ***, $p<0.001$; Wilcoxon rank-sum test.
496 **(L-O)** Time-lapse imaging of Ca^{2+} signaling in cultured wing discs. The calcium
497 reporter GCaMP6m (shown in pseudo color) was expressed in the wing pouch of wild-
498 type (L), *RpS3/+* (M), or *RpS3/+, nub-Gal4, UAS-Puc* (N) flies. Images were acquired
499 at 10-second intervals. White arrowheads indicate the persistent activation of Ca^{2+}
500 signaling. White asterisks indicate spontaneous Ca^{2+} flashes. The images correspond to
501 the boxed area in the schematic diagram of the wing disc (O). Scale bar, 5 μm.
502 **(P)** Quantification of cells exhibiting continuous Ca^{2+} activity for 20 minutes in the
503 wing pouch. The respective genotypes are shown in (L) (n=12), (M) (n=10) or (N) (n=9).
504 These images are Z-stacked images from 3 confocal images (4μm). Arrowheads
505 indicate massive cell death in the Error bars, SEM; **, $p<0.01$; Wilcoxon rank-sum test.
506

507

508 **Fig 2. Exocytosis is required for massive cell-turnover in the *M/+* wing pouch**

509 **(A-E)** Wing discs of wild-type (A), *RpS3/+* (B), *RpS3/+, nub-Gal4, UAS-Puc* (C),
510 *RpS3/+, nub-Gal4, UAS-unc-13-RNAi* (D) or *RpS3/+, nub-Gal4, UAS-Rab3-RNAi* (E)
511 flies were stained with anti-phospho-histone H3 (pH3) (Ser10) antibody (white). Wing
512 pouches were marked in pale green. Scale bar, 100 μm.

513 **(F-J)** The activated-caspase-3 indicator CD8-PARP-Venus was expressed in the wing
514 pouch of wild-type (F), *RpS3/+, nub-Gal4, UAS-lexA-RNAi* (G), *RpS3/+, nub-Gal4,*
515 *UAS-unc-13-RNAi* (H), *RpS3/+, nub-Gal4, UAS-Rab3-RNAi* (I), or *RpS3/+, nub-Gal4,*
516 *UAS-SNAP25-RNAi* (J) flies, and dying cells in the wing pouch were visualized by anti-
517 cleaved PARP staining (white). Orange arrowheads indicate massive cell death in the
518 *RpS3/+* wing pouch. Scale bar, 100μm.

519 **(L)** Adult wing phenotypes were classified as following five types: (a) normal, (b) vein
520 (weak) (weakly bearing a brunched vein in the point of "landmark 14" (arrow) (65) (c)
521 vein (strong) (bearing other additional vein phenotypes (arrowheads) in addition to
522 "landmark 14"), (d) notch, and (e) severe.

523 **(K)** The rate of defective wings in the genotypes of wild-type (n=55), *RpS3/+* (n=44),
524 *RpS3/+, nub-Gal4, UAS-Puc* (n=63), *RpS3/+, nub-Gal4, UAS-unc-13-RNAi* (n=101)
525 and *RpS3/+, nub-Gal4, UAS-Rab3-RNAi* (n=99).

526 **(M-O')** Using *puc-gal4* driver, CD8-PARP-Venus (white) was expressed in JNK-
527 activating cells in the wing disc of wild-type (M), *RpS3/+,* (N) or *RpS3/+, UAS-Rab3-*
528 *RNAi* (O) flies. Dying cells in the JNK-activating cells were visualized by anti-cleaved
529 PARP staining (white). Scale bar, 100μm.

530 **(P)** Boxplot with individual dots representing pH3-positive areas in the pouch of
531 genotypes shown in (A) (n=18), (B) (n=22), (C) (n=23), (D) (n=12) and (E) (n=21).
532 Error bars, SEM; ***, $p<0.001$; Wilcoxon rank-sum test.

533 **(Q)** Boxplot with individual dots representing the number of cleaved-PARP-positive
534 dying cells per pouch in genotypes shown in (F) (n=18), (G) (n=24), (H) (n=18), (I)
535 (n=13), and (J) (n=13). Error bars, SEM; ***, $p<0.001$, *, $p<0.05$; Wilcoxon rank-sum
536 test.

537 **(R)** Boxplot with individual dots representing the number of cleaved-PARP-positive
538 dying cells in JNK-activating cells per pouch. The respective genotypes are shown in

539 (M) (n=16), (N) (n=21), and (O) (n=23). Error bars, SEM; ***, p<0.001; Wilcoxon
540 rank-sum test.
541
542
543 **Fig 3. Dying cells secrete Wg via exocytosis in the *M/+* wing pouch**
544 **(A-C')** Wg expression was visualized by anti-Wg staining (white) in the wing pouch of
545 *nub-Gal4, UAS-p35* (A), *RpS3/+, nub-Gal4, UAS-p35* (B), or *RpS3/+, nub-Gal4, UAS-*
546 *p35*, *UAS-Puc* (C) flies. The nuclei were visualized by DAPI staining (white). Scale
547 bar, 100μm.
548 **(D-E''')** Immunofluorescent localization of the exosome marker CD63-mCherry, as
549 visualized by anti-dsRed staining (magenta), and GFP-Wingless (white) in the wing
550 pouch of *GFP-Wg/+* (D) or *RpS3/+*, *GFP-Wg/+* (E) flies expressing CD63-mCherry.
551 The nuclei were visualized by DAPI staining (blue). The images correspond to the area
552 enclosed by rectangle 1 in the schematic diagram of the wing disc (F). Orange
553 arrowheads indicate the colocalization of GFP-Wingless-positive puncta with CD63-
554 mCherry-positive puncta. Scale bar, 20μm.
555 **(G-J')** The membrane-tethered anti-GFP nanobody (Vhh4-CD8-HA) was expressed in
556 the wing pouch of *GFP-Wg/+* (G), *RpS3/+*, *GFP-Wg/+* (H), *RpS3/+*, *GFP-Wg/+*, *nub-*
557 *Gal4, UAS-Puc* (I), or *RpS3/+*, *GFP-Wg/+*, *nub-Gal4, UAS-unc-13-RNAi* (J) flies.
558 GFP-Wingless was visualized by anti-GFP staining (white). The nuclei were visualized
559 by DAPI staining (white). The images correspond to the area enclosed by the rectangle
560 2 in the schematic diagram of the wing disc (F). Immobilized Wg-GFP-positive puncta
561 were frequently observed in the area of morphological dying cells in the *RpS3/+* wing
562 pouch (Indicated by orange arrowheads). Scale bar, 50μm.
563 **(K)** Boxplot with individual dots representing the number of GFP-Wingless-positive
564 puncta per rectangle-2 in the wing pouch (F). The respective genotypes are shown in
565 (G) (n=9), (H) (n=14), (I)(n=11), and (J) (n=11). Error bars, SEM; ***, p<0.001, **,
566 p<0.01; Wilcoxon rank-sum test.
567
568
569 **Fig 4. Fz2 contributes to massive cell-turnover in the *M/+* wing pouch**
570 **(A-D''')** The expression of *fz2* in the wing disc of *fz2-lacZ/+* (A), *RpS3/+*, *fz2-lacZ/+*
571 (B), or *RpS3/+*, *fz2-lacZ/+, nub-Gal4, UAS-Puc* (D) flies was visualized by anti-β-

572 galactosidase staining (white). Dying cells in the wing disc were visualized by anti-
573 cleaved Dcp-1 staining (magenta). The nuclei were visualized by DAPI staining (blue).
574 (C)–(C'''') are high-magnification images of the boxed area in (B)–(B'''). Orange
575 arrowheads in (B-C'''') indicate dying cells that exhibit relatively lower *fz2* expression
576 compared to their surrounding cells.
577 **(F)** Average fluorescence intensities of *Fz2-lacZ* along the dorsal compartment (as
578 indicated the pale yellow area in (E)). Each line represents the average intensity in either
579 *fz2-lacZ/+* (n=6) (blue) or *RpS3/+, fz2-lacZ/+* (n=6) (red) flies.
580 **(G-I)** Dying cells were visualized by anti-cleaved PARP staining in the wing pouch of
581 *RpS3/+, nub-Gal4, UAS-fz2-RNAi* (9739R-1) (G), *RpS3/+, nub-Gal4, UAS-fz2-RNAi*
582 (9739R-2) (H), or *RpS3/+, fz2/+* (I) flies expressing CD8-PARP-Venus (white). Scale
583 bar, 100μm.
584 **(J)** Boxplot with individual dots representing the number of cleaved-PARP-positive
585 dying cells per pouch. The respective genotypes are shown in (Fig 2G) (n=24, number
586 of wing pouches), (G) (n=22), (H) (n=25), and (I) (n=19). Error bars, SEM; ***,
587 p<0.001; Wilcoxon rank-sum test.
588 **(K)** Wing discs of *RpS3/+, nub-Gal4, UAS-fz2-RNAi* flies were stained with anti-
589 phospho-histone H3 (pH3) (Ser10) antibody (white). Wing pouches were marked in
590 pale green. Scale bar, 100μm.
591 **(L)** Boxplot with individual dots representing pH3-positive areas in the pouch of
592 genotypes shown in (2A) (n=18, number of wing pouches), (2B) (n=22), and (K) (n=21).
593 Error bars, SEM; ***, p<0.001, **, p<0.01; Wilcoxon rank-sum test.
594
595
596 **Fig 5. A model for ensuring robust coordination of tissue growth in *M*/+ animals**
597 During the larval period of *M*/+ animals, JNK signaling is activated in the *M*/+ wing
598 pouch, which induces the expression of exocytosis-related genes and Wg, leading to
599 the secretion of Wg through exocytosis in dying cells. Subsequently, neighboring cells
600 then receive Wg via Fz2 receptor, establishing their apoptosis/proliferative status and
601 consequently leading to massive cell-turnover in the *M*/+ wing pouch.
602
603
604 **Supporting information**

605

606 **S1 Fig, related to Figure 1. *M/+* wing pouch elevates exocytosis downstream of**
607 **JNK signaling.**

608 **(A)** Schematic representation of the genotypes used for transcriptional profiling:
609 mRNA was isolated from FACS-Sorted GFP^+ pouch cells (green) in third instar wing
610 discs of wild-type, *RpS3*/+, or *RpS3*/+, *nub-Gal4, UAS-Puc* flies.

611 **(B)** Four GO terms for biological process were significantly enriched in the *RpS3/+*-
612 regulated genes.

613 **(C)** Venn diagram depicting genes that are differentially expressed in *RpS3*/+ cells
614 compared to wild-type cells, with 362 of these changes being regulated by JNK
615 signaling.

616 **(D)** Expression levels (fold changes relative to wild-type control or *RpS3*/+, *nub-Gal4,*
617 *UAS-Puc*) for *RpS3*/+ -regulated genes associated with the "secretion by cell" GO term.
618 These genes were regulated by JNK signaling in the *RpS3/+* wing pouch.

619 **(E)** EGFP-CD63 was expressed in the wing pouch of *RpL19/+* flies (white). Dying
620 cells were visualized by anti-cleaved Dcp-1 staining in the wing discs (white).
621 Arrowheads indicate massive cell death in the *RpS3/+* wing pouch. Scale bar, 50 μm.

622 **(F)** Boxplot with individual dots representing the number of EGFP-CD63-positive
623 puncta in the pouch of genotypes shown in Fig.1(A) (n=13, number of wing pouches)
624 and Fig S1(E) (n=13). Error bars, SEM; ***, $p<0.001$; Wilcoxon rank-sum test.

625 **(G-H')** Wing discs of wild-type (G) or *RpS3/+* (H) flies were stained with anti-Hrs
626 antibody (white). The nuclei were visualized by DAPI staining (blue). Hrs-positive
627 vesicles were frequently observed in the area of morphological dying cells in the
628 *RpS3/+* wing pouch (Indicated by orange arrowheads). The images correspond to the
629 area enclosed by rectangle 1 in the schematic diagram of the wing disc (Fig S3B). Scale
630 bar, 20μm.

631 **(I)** Boxplot with individual dots representing the number of Hrs-positive puncta in the
632 pouch of genotypes shown in Fig.S1(G) (n=14, number of wing pouches) and
633 Fig.S1(H) (n=14). Error bars, SEM; ***, $p<0.001$; Wilcoxon rank-sum test.

634

635 **S2 Fig, related to Figure 2. Exocytosis is required for massive cell-turnover in**
636 **the *M/+* wing pouch.**

637 **(A-J)** CD8-PARP-Venus was expressed in the wing pouch of *RpS3/+, nub-Gal4, UAS-*
638 *Puc* (A), *RpS3/+, nub-Gal4, UAS-unc-13-RNAi* (B), *RpS3/+, nub-Gal4, UAS-Rab3-*
639 *RNAi* (C), *RpS3/+, nub-Gal4, UAS-SNAP25-RNAi* (D), *RpS3/+, nub-Gal4, UAS-Syt-*
640 *RNAi* (E and F), *RpS3/+, nub-Gal4, UAS-Rab27-RNAi* (G and H), or *RpS3/+, nub-Gal4,*
641 *UAS-ALiX-RNAi* (I and J) flies, and dying cells in the wing pouch were visualized by
642 anti-cleaved PARP staining (white). Scale bar, 100μm.
643 **(K)** The rate of defective wings in the genotypes of *nub-Gal4, UAS-Puc* (n=41), *nub-*
644 *Gal4, UAS-unc-13-RNAi* (n=55) and *nub-Gal4, UAS-Rab3-RNAi* (n=61).
645 **(L-M')** Using *puc-gal4* driver, CD8-PARP-Venus (white) was expressed in JNK-
646 activating cells in the wing disc of *RpL19/+,* (L) or *RpL19/+, puc-Gal4, UAS-Rab3-*
647 *RNAi* (M). Dying cells in the JNK-activating cells were visualized by anti-cleaved
648 PARP staining (white). Scale bar, 100 μm. Scale bar, 100μm.
649 **(N)** Boxplot with individual dots representing the number of cleaved-PARP-positive
650 dying cells per pouch in genotypes shown in (Fig 2F) (n=18), (Fig 2G) (n=24), (A)
651 (n=18), (B) (n=14), (C) (n=13), (D (n=12), (E) (n=15), (F) (n=10), (G) (n=13), (H)
652 (n=14), (I) (n=13), and (J) (n=13). Error bars, SEM; ***, $p<0.001$, **, $p<0.01$;
653 Wilcoxon rank-sum test.
654 **(O)** Boxplot with individual dots representing the number of cleaved-PARP-positive
655 dying cells in JNK-activating cells per pouch. The respective genotypes are shown in
656 (L) (n=11), and (M) (n=9). Error bars, SEM; ***, $p<0.001$; Wilcoxon rank-sum test.
657
658 **S3 Fig, related to Figure 3. Dying cells Secrete Wg via exocytosis in the M/+ wing**
659 **pouch.**
660 **(A-B)** Relative position of dying cells (cleaved PARP, magenta) and Wg signaling
661 activity (anti-β-galactosidase, white) in the wing pouch of *RpS3/+, nmo-LacZ/+* flies
662 (A). Orange arrowheads in (A-A''') indicate dying cells that exhibit relatively lower
663 Wg activity compared to their surrounding cells. The nuclei were visualized by DAPI
664 staining (blue). The images correspond to the area enclosed by rectangle 1 in the
665 schematic diagram of the wing disc (B). Scale bar, 50μm.
666 **(C)** CD63-mcherry and Vhh4-CD8-HA were expressed in the wing pouch of *RpS3/+,*
667 *GFP-Wg/+* flies. CD63-mCherry was visualized by anti-dsRed staining (magenta).
668 GFP-Wingless was visualized by anti-GFP staining (white). The nuclei were visualized
669 by DAPI staining (blue). Orange arrowheads indicate the colocalization between

670 CD63-mCherry-positive and GFP-Wingless-positive puncta. The images correspond to
671 the area enclosed by rectangle 2 in the schematic diagram of the wing disc (B). Scale
672 bar, 20μm.
673 **(D-E'''**) Vhh4-CD8-HA was expressed in the wing pouch of *GFP-Wg/+* (D) or *RpS3/+*,
674 *GFP-Wg/+* (E) flies. Extracellular CD63-mCherry and extracellular GFP-Wingless
675 were visualized by anti-dsRed staining (magenta) and anti-GFP staining (white),
676 respectively. The nuclei were visualized by DAPI staining (blue). Orange arrowheads
677 indicate the colocalization of extracellular GFP-Wingless-positive puncta with
678 extracellular CD63-mCherry-positive puncta. The images correspond to the area
679 enclosed by the rectangle 2 in the schematic diagram of the wing disc (B). Scale bar,
680 20μm.
681 **(F)** Boxplot with individual dots representing extracellular CD63-mCherry-positive
682 area in the region enclosed by rectangle 2 in the schematic diagram of the wing disc
683 (B). The respective genotypes are shown in (D) (n=10) and (E) (n=12). Error bars,
684 SEM; *, $p<0.05$; Wilcoxon rank-sum test.
685 **(G)** Boxplot with individual dots representing extracellular GFP-Wingess-positive area
686 in the region enclosed by rectangle 2 in the schematic diagram of the wing disc (B).
687 The respective genotypes are shown in (D) (n=10), and (E) (n=12) Error bars, SEM;
688 ***, $p<0.001$; Wilcoxon rank-sum test.
689
690
691 **S4 Fig, related to Figure 4. Fz2 contributes to massive cell-turnover in the *M/+***
692 **wing pouch.**
693 **(A-D'''**) The expression of Fz2 in the wing disc of *fz2-Venus/+* (A), *RpS3/+*, *fz2-*
694 *Venus/+* (B), or *RpS3/+*, *fz2-Venus/+, nub-Gal4, UAS-Puc* (D) flies was visualized by
695 anti-GFP staining (white). Dying cells in the wing disc were visualized by anti-cleaved
696 Dcp-1 staining (magenta). The nuclei were visualized by DAPI staining (blue). (C)–
697 (C''') are high-magnification images of the boxed area in (B)–(B'''). Orange
698 arrowheads in (B-C''') indicate dying cells that exhibit relatively lower Fz2 expression
699 compared to their surrounding cells.
700
701 **S1 Movie. Calcium Time-lapse imaging of wing discs**

The calcium reporter GCaMP6m was expressed in wing pouches of wild-type larvae. Wing discs were dissected and subjected to time-lapse imaging at 10-second intervals with a Leica STELLARIS confocal microscope. See *Methods* for details.

S2 Movie. Calcium Time-lapse imaging of wing discs

The calcium reporter GCaMP6m was expressed in wing pouches of *RpS3/+* larvae. Wing discs were dissected and subjected to time-lapse imaging at 10-second intervals with a Leica STELLARIS confocal microscope. See *Methods* for details.

S3 Movie. Calcium Time-lapse imaging of wing discs

The calcium reporter GCaMP6m was expressed in wing pouches of *RpS3/+*, *nub-Gal4, UAS-Puc* larvae. Wing discs were dissected and subjected to time-lapse imaging at 10-second intervals with a Leica STELLARIS confocal microscope. See *Methods* for details.

S1 Table

List of genes identified as differentially expressed by RNA-seq between RpS3/+ and WT, and between RpS3/+, +Puc and WT pouch cells.

S2 Table

List of genes identified as differentially expressed by RNA-seq between *RpS3*/+ and *RpS3*/+, +Puc pouch cells.

S3 Table

List of genes differentially expressed in *RpS3*/+ pouch cells, associated with JNK or JAK/STAT targets, Gr64 gustatory receptors, oxidative stress, and DNA repair.

S4 Table

Summary of statistical analysis.

S1 Text

Detailed Genotypes used in each figure.

References

1. Cmejla R, Cmejlova J, Handrkova H, Petrak J, Pospisilova D. Ribosomal protein S17 gene (RPS17) is mutated in Diamond-Blackfan anemia. Hum Mutat. 2007;28(12):1178-82.

2. Doherty L, Sheen MR, Vlachos A, Choesmel V, O'Donohue MF, Clinton C, et al. Ribosomal protein genes RPS10 and RPS26 are commonly mutated in Diamond-Blackfan anemia. Am J Hum Genet. 2010;86(2):222-8.

3. Campagnoli MF, Ramenghi U, Armiraglio M, Quarello P, Garelli E, Carando A, et al. RPS19 mutations in patients with Diamond-Blackfan anemia. Hum Mutat. 2008;29(7):911-20.

4. Choesmel V, Fribourg S, Aguissa-Touré AH, Pinaud N, Legrand P, Gazda HT, et al. Mutation of ribosomal protein RPS24 in Diamond-Blackfan anemia results in a ribosome biogenesis disorder. Hum Mol Genet. 2008;17(9):1253-63.

5. Wang R, Yoshida K, Toki T, Sawada T, Uechi T, Okuno Y, et al. Loss of function mutations in RPL27 and RPS27 identified by whole-exome sequencing in Diamond-Blackfan anaemia. Br J Haematol. 2015;168(6):854-64.

6. Danilova N, Gazda HT. Ribosomopathies: how a common root can cause a tree of pathologies. Dis Model Mech. 2015;8(9):1013-26.

7. Lipton JM, Ellis SR. Diamond-Blackfan anemia: diagnosis, treatment, and molecular pathogenesis. Hematol Oncol Clin North Am. 2009;23(2):261-82.

8. Bolze A, Mahlaoui N, Byun M, Turner B, Trede N, Ellis SR, et al. Ribosomal protein SA haploinsufficiency in humans with isolated congenital asplenia. Science. 2013;340(6135):976-8.

9. Brehme KS. A Study of the Effect on Development of "Minute" Mutations in Drosophila Melanogaster. Genetics. 1939;24(2):131-61.

10. Recasens-Alvarez C, Alexandre C, Kirkpatrick J, Nojima H, Huels DJ, Snijders AP, et al. Ribosomopathy-associated mutations cause proteotoxic stress that is alleviated by TOR inhibition. Nat Cell Biol. 2021;23(2):127-35.

11. Baumgartner ME, Dinan MP, Langton PF, Kucinski I, Piddini E. Proteotoxic stress is a driver of the loser status and cell competition. Nat Cell Biol. 2021;23(2):136-46.

12. Kucinski I, Dinan M, Kolahgar G, Piddini E. Chronic activation of JNK JAK/STAT and oxidative stress signalling causes the loser cell status. Nat Commun. 2017;8(1):136.

13. Lee CH, Kiparaki M, Blanco J, Folgado V, Ji Z, Kumar A, et al. A Regulatory Response to Ribosomal Protein Mutations Controls Translation, Growth, and Cell Competition. Dev Cell. 2018;46(4):456-69.e4.

774 14. Akai N, Ohsawa S, Sando Y, Igaki T. Epithelial cell-turnover ensures robust
775 coordination of tissue growth in Drosophila ribosomal protein mutants. PLoS Genet.
776 2021;17(1):e1009300.

777 15. Fan Y, Bergmann A. Distinct mechanisms of apoptosis-induced compensatory
778 proliferation in proliferating and differentiating tissues in the Drosophila eye. Dev Cell.
779 2008;14(3):399-410.

780 16. Pérez-Garijo A, Martín FA, Morata G. Caspase inhibition during apoptosis causes
781 abnormal signalling and developmental aberrations in Drosophila. Development.
782 2004;131(22):5591-8.

783 17. Ryoo HD, Gorenc T, Steller H. Apoptotic cells can induce compensatory cell
784 proliferation through the JNK and the Wingless signaling pathways. Dev Cell.
785 2004;7(4):491-501.

786 18. Smith-Bolton RK, Worley MI, Kanda H, Hariharan IK. Regenerative growth in
787 Drosophila imaginal discs is regulated by Wingless and Myc. Dev Cell.
788 2009;16(6):797-809.

789 19. Morata G, Ripoll P. Minutes: mutants of drosophila autonomously affecting cell
790 division rate. Dev Biol. 1975;42(2):211-21.

791 20. Ogawa M, Kawarazaki Y, Fujita Y, Naguro I, Ichijo H. FGF21 Induced by the
792 ASK1-p38 Pathway Promotes Mechanical Cell Competition by Attracting Cells. Curr
793 Biol. 2021;31(5):1048-57.e5.

794 21. Aravamudan B, Fergestad T, Davis WS, Rodesch CK, Broadie K. Drosophila
795 UNC-13 is essential for synaptic transmission. Nat Neurosci. 1999;2(11):965-71.

796 22. Megighian A, Scorzeto M, Zanini D, Pantano S, Rigoni M, Benna C, et al. Arg206
797 of SNAP-25 is essential for neuroexocytosis at the Drosophila melanogaster
798 neuromuscular junction. J Cell Sci. 2010;123(Pt 19):3276-83.

799 23. Renden R, Berwin B, Davis W, Ann K, Chin CT, Kreber R, et al. Drosophila
800 CAPS is an essential gene that regulates dense-core vesicle release and synaptic vesicle
801 fusion. Neuron. 2001;31(3):421-37.

802 24. Omar-Hmeadi M, Idevall-Hagren O. Insulin granule biogenesis and exocytosis.
803 Cell Mol Life Sci. 2021;78(5):1957-70.

804 25. Eugster C, Panáková D, Mahmoud A, Eaton S. Lipoprotein-heparan sulfate
805 interactions in the Hh pathway. Dev Cell. 2007;13(1):57-71.

806 26. Gross JC, Chaudhary V, Bartscherer K, Boutros M. Active Wnt proteins are
807 secreted on exosomes. Nat Cell Biol. 2012;14(10):1036-45.

808 27. Panáková D, Sprong H, Marois E, Thiele C, Eaton S. Lipoprotein particles are
809 required for Hedgehog and Wingless signalling. Nature. 2005;435(7038):58-65.

810 28. Redhai S, Hellberg JE, Wainwright M, Perera SW, Castellanos F, Kroeger B, et
811 al. Regulation of Dense-Core Granule Replenishment by Autocrine BMP Signalling in
812 Drosophila Secondary Cells. PLoS Genet. 2016;12(10):e1006366.

813 29. Sugita S, Han W, Butz S, Liu X, Fernández-Chacón R, Lao Y, et al.
814 Synaptotagmin VII as a plasma membrane Ca(2+) sensor in exocytosis. Neuron.
815 2001;30(2):459-73.

816 30. Yamanaka N, Marqués G, O'Connor MB. Vesicle-Mediated Steroid Hormone
817 Secretion in Drosophila melanogaster. Cell. 2015;163(4):907-19.

818 31. Zhang YQ, Rodesch CK, Broadie K. Living synaptic vesicle marker:
819 synaptotagmin-GFP. Genesis. 2002;34(1-2):142-5.

820 32. Chen TW, Wardill TJ, Sun Y, Pulver SR, Renninger SL, Baohan A, et al.
821 Ultrasensitive fluorescent proteins for imaging neuronal activity. Nature.
822 2013;499(7458):295-300.

823 33. Enomoto M, Kizawa D, Ohsawa S, Igaki T. JNK signaling is converted from anti-
824 to pro-tumor pathway by Ras-mediated switch of Warts activity. Dev Biol.
825 2015;403(2):162-71.

826 34. Florentin A, Arama E. Caspase levels and execution efficiencies determine the
827 apoptotic potential of the cell. J Cell Biol. 2012;196(4):513-27.

828 35. Gorelick-Ashkenazi A, Weiss R, Sapozhnikov L, Florentin A, Tarayrah-Ibraheim
829 L, Dweik D, et al. Caspases maintain tissue integrity by an apoptosis-independent
830 inhibition of cell migration and invasion. Nat Commun. 2018;9(1):2806.

831 36. Liang CJ, Chang YC, Chang HC, Wang CK, Hung YC, Lin YE, et al. Derlin-1
832 regulates mutant VCP-linked pathogenesis and endoplasmic reticulum stress-induced
833 apoptosis. PLoS Genet. 2014;10(9):e1004675.

834 37. Ohsawa S, Sato Y, Enomoto M, Nakamura M, Betsumiya A, Igaki T.
835 Mitochondrial defect drives non-autonomous tumour progression through Hippo
836 signalling in Drosophila. Nature. 2012;490(7421):547-51.

837 38. Ohsawa S, Sugimura K, Takino K, Xu T, Miyawaki A, Igaki T. Elimination of
838 oncogenic neighbors by JNK-mediated engulfment in Drosophila. Dev Cell.
839 2011;20(3):315-28.

840 39. Shinoda N, Obata F, Zhang L, Miura M. Drosophila SETDB1 and caspase
841 cooperatively fine-tune cell fate determination of sensory organ precursor. Genes Cells.
842 2016;21(4):378-86.

843 40. Williams DW, Kondo S, Krzyzanowska A, Hiromi Y, Truman JW. Local caspase
844 activity directs engulfment of dendrites during pruning. Nat Neurosci.
845 2006;9(10):1234-6.

846 41. de Wit H, Walter AM, Milosevic I, Gulyás-Kovács A, Riedel D, Sørensen JB, et
847 al. Synaptotagmin-1 docks secretory vesicles to syntaxin-1/SNAP-25 acceptor
848 complexes. Cell. 2009;138(5):935-46.

849 42. Baietti MF, Zhang Z, Mortier E, Melchior A, Degeest G, Geeraerts A, et al.
850 Syndecan-syntenin-ALIX regulates the biogenesis of exosomes. Nat Cell Biol.
851 2012;14(7):677-85.

852 43. Ghossoub R, Lembo F, Rubio A, Gaillard CB, Bouchet J, Vitale N, et al. Syntenin-
853 ALIX exosome biogenesis and budding into multivesicular bodies are controlled by
854 ARF6 and PLD2. Nat Commun. 2014;5:3477.

855 44. Vincent JP, Kolahgar G, Gagliardi M, Piddini E. Steep differences in wingless
856 signaling trigger Myc-independent competitive cell interactions. Dev Cell.
857 2011;21(2):366-74.

858 45. Beckett K, Monier S, Palmer L, Alexandre C, Green H, Bonneil E, et al.
859 Drosophila S2 cells secrete wingless on exosome-like vesicles but the wingless gradient
860 forms independently of exosomes. Traffic. 2013;14(1):82-96.

861 46. Koles K, Nunnari J, Korkut C, Barria R, Brewer C, Li Y, et al. Mechanism of
862 evenness interrupted (Evi)-exosome release at synaptic boutons. J Biol Chem.
863 2012;287(20):16820-34.

864 47. Korkut C, Ataman B, Ramachandran P, Ashley J, Barria R, Gherbesi N, et al.
865 Trans-synaptic transmission of vesicular Wnt signals through Evi/Wntless. Cell.
866 2009;139(2):393-404.

867 48. Won JH, Cho KO. Wg secreted by conventional Golgi transport diffuses and forms
868 Wg gradient whereas Wg tethered to extracellular vesicles do not diffuse. Cell Death
869 Differ. 2021;28(3):1013-25.

870 49. Cordero JB, Stefanatos RK, Scopelliti A, Vidal M, Sansom OJ. Inducible
871 progenitor-derived Wingless regulates adult midgut regeneration in Drosophila. Embo
872 j. 2012;31(19):3901-17.

873 50. Pérez-Garijo A, Shlevkov E, Morata G. The role of Dpp and Wg in compensatory
874 proliferation and in the formation of hyperplastic overgrowths caused by apoptotic cells
875 in the Drosophila wing disc. Development. 2009;136(7):1169-77.

876 51. McGough IJ, Vecchia L, Bishop B, Malinauskas T, Beckett K, Joshi D, et al.
877 Glypicans shield the Wnt lipid moiety to enable signalling at a distance. Nature.
878 2020;585(7823):85-90.

879 52. Bhanot P, Brink M, Samos CH, Hsieh JC, Wang Y, Macke JP, et al. A new
880 member of the frizzled family from Drosophila functions as a Wingless receptor. Nature.
881 1996;382(6588):225-30.

882 53. Cadigan KM, Fish MP, Rulifson EJ, Nusse R. Wingless repression of Drosophila
883 frizzled 2 expression shapes the Wingless morphogen gradient in the wing. Cell.
884 1998;93(5):767-77.

885 54. Huelsken J, Behrens J. The Wnt signalling pathway. J Cell Sci. 2002;115(Pt
886 21):3977-8.

887 55. Lawrence PA, Casal J, Struhl G. Towards a model of the organisation of planar
888 polarity and pattern in the Drosophila abdomen. Development. 2002;129(11):2749-60.

889 56. Lowe N, Rees JS, Roote J, Ryder E, Armean IM, Johnson G, et al. Analysis of the
890 expression patterns, subcellular localisations and interaction partners of Drosophila
891 proteins using a pigP protein trap library. Development. 2014;141(20):3994-4005.

892 57. Lye CM, Naylor HW, Sanson B. Subcellular localisations of the CPTI collection
893 of YFP-tagged proteins in Drosophila embryos. Development. 2014;141(20):4006-17.

894 58. Fogarty CE, Bergmann A. Killers creating new life: caspases drive apoptosis-
895 induced proliferation in tissue repair and disease. Cell Death Differ. 2017;24(8):1390-
896 400.

897 59. Morata G, Shlevkov E, Pérez-Garijo A. Mitogenic signaling from apoptotic cells
898 in Drosophila. Dev Growth Differ. 2011;53(2):168-76.

899 60. Su TT. Non-autonomous consequences of cell death and other perks of being
900 metazoan. AIMS Genet. 2015;2(1):54-69.

901 61. Fan Y, Wang S, Hernandez J, Yenigun VB, Hertlein G, Fogarty CE, et al. Genetic
902 models of apoptosis-induced proliferation decipher activation of JNK and identify a
903 requirement of EGFR signaling for tissue regenerative responses in Drosophila. PLoS
904 Genet. 2014;10(1):e1004131.

905 62. Chen Q, Takada R, Noda C, Kobayashi S, Takada S. Different populations of Wnt-
906 containing vesicles are individually released from polarized epithelial cells. Sci Rep.
907 2016;6:35562.

908 63. Mulligan KA, Fuerer C, Ching W, Fish M, Willert K, Nusse R. Secreted Wingless-
909 interacting molecule (Swim) promotes long-range signaling by maintaining Wingless
910 solubility. Proc Natl Acad Sci U S A. 2012;109(2):370-7.

911 64. Xue S, Barna M. Specialized ribosomes: a new frontier in gene regulation and
912 organismal biology. Nat Rev Mol Cell Biol. 2012;13(6):355-69.

913 65. Martín-Blanco E, Gampel A, Ring J, Virdee K, Kirov N, Tolkovsky AM, et al.
914 puckered encodes a phosphatase that mediates a feedback loop regulating JNK activity
915 during dorsal closure in Drosophila. Genes Dev. 1998;12(4):557-70.

916 66. Hay BA, Wolff T, Rubin GM. Expression of baculovirus P35 prevents cell death
917 in Drosophila. Development. 1994;120(8):2121-9.

918 67. Chen CM, Struhl G. Wingless transduction by the Frizzled and Frizzled2 proteins
919 of Drosophila. Development. 1999;126(23):5441-52.

920 68. Aldaz S, Escudero LM, Freeman M. Live imaging of Drosophila imaginal disc
921 development. Proceedings of the National Academy of Sciences of the United States of
922 America. 2010;107(32):14217-22.

923 69. Iida C, Ohsawa S, Taniguchi K, Yamamoto M, Morata G, Igaki T. JNK-mediated
924 Slit-Robo signaling facilitates epithelial wound repair by extruding dying cells.
925 Scientific reports. 2019;9(1):19549.

926 70. Cong B, Nakamura M, Sando Y, Kondo T, Ohsawa S, Igaki T. JNK and Yorkie
927 drive tumor malignancy by inducing L-amino acid transporter 1 in Drosophila. PLoS
928 Genet. 2021;17(11):e1009893.

929 71. Dobin A, Davis CA, Schlesinger F, Drenkow J, Zaleski C, Jha S, et al. STAR:
930 ultrafast universal RNA-seq aligner. Bioinformatics. 2013;29(1):15-21.

931 72. Li B, Dewey CN. RSEM: accurate transcript quantification from RNA-Seq data
932 with or without a reference genome. BMC Bioinformatics. 2011;12:323.

933 73. Robinson MD, McCarthy DJ, Smyth GK. edgeR: a Bioconductor package for
934 differential expression analysis of digital gene expression data. Bioinformatics.
935 2010;26(1):139-40.
936

Akai *et al.*, Fig 1

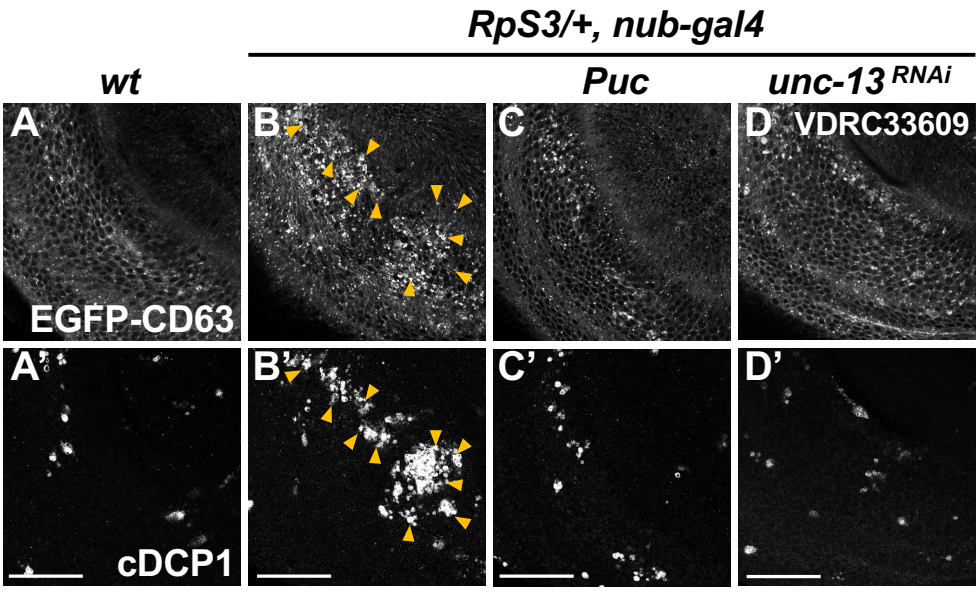

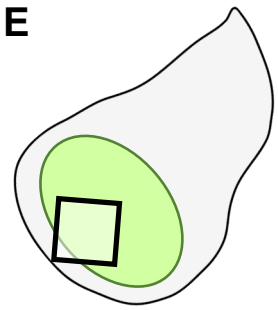

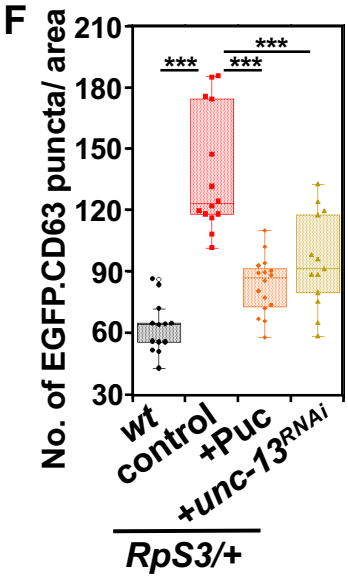

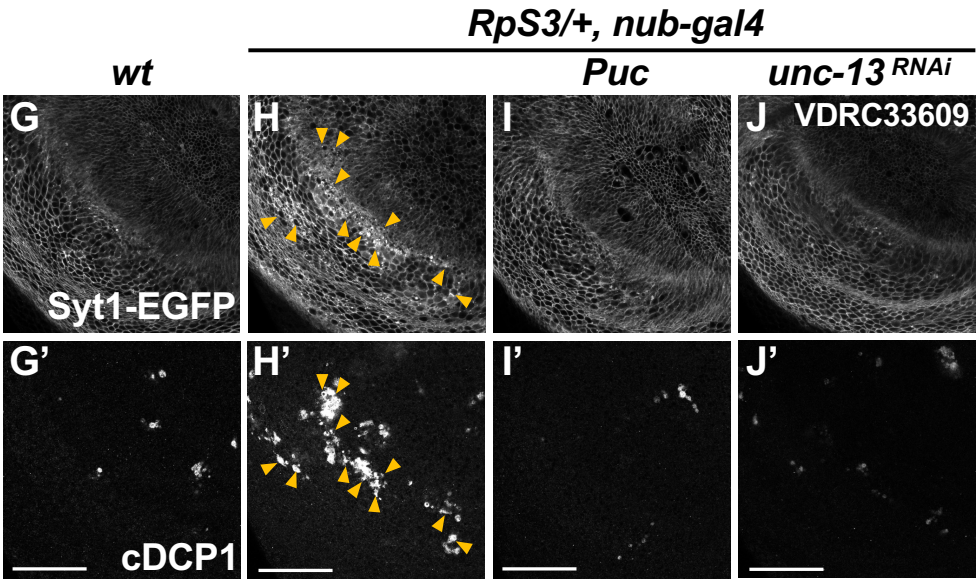

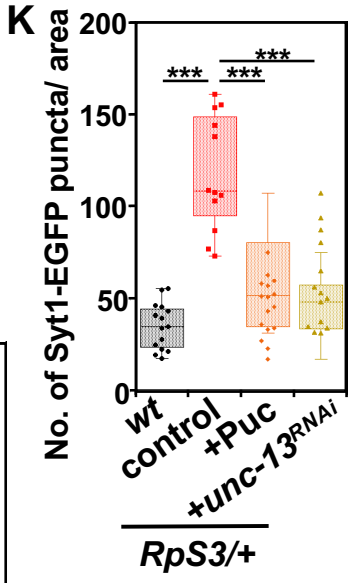

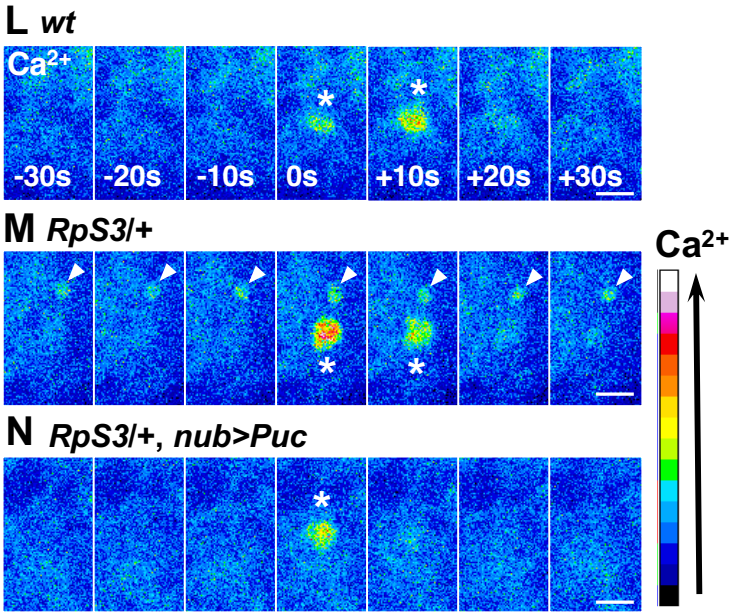

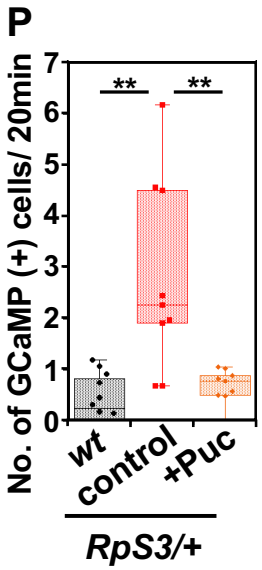

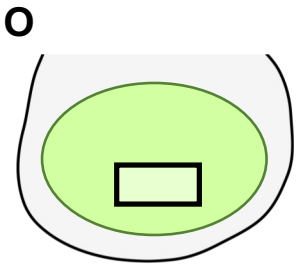

Akai *et al.*, Fig 2

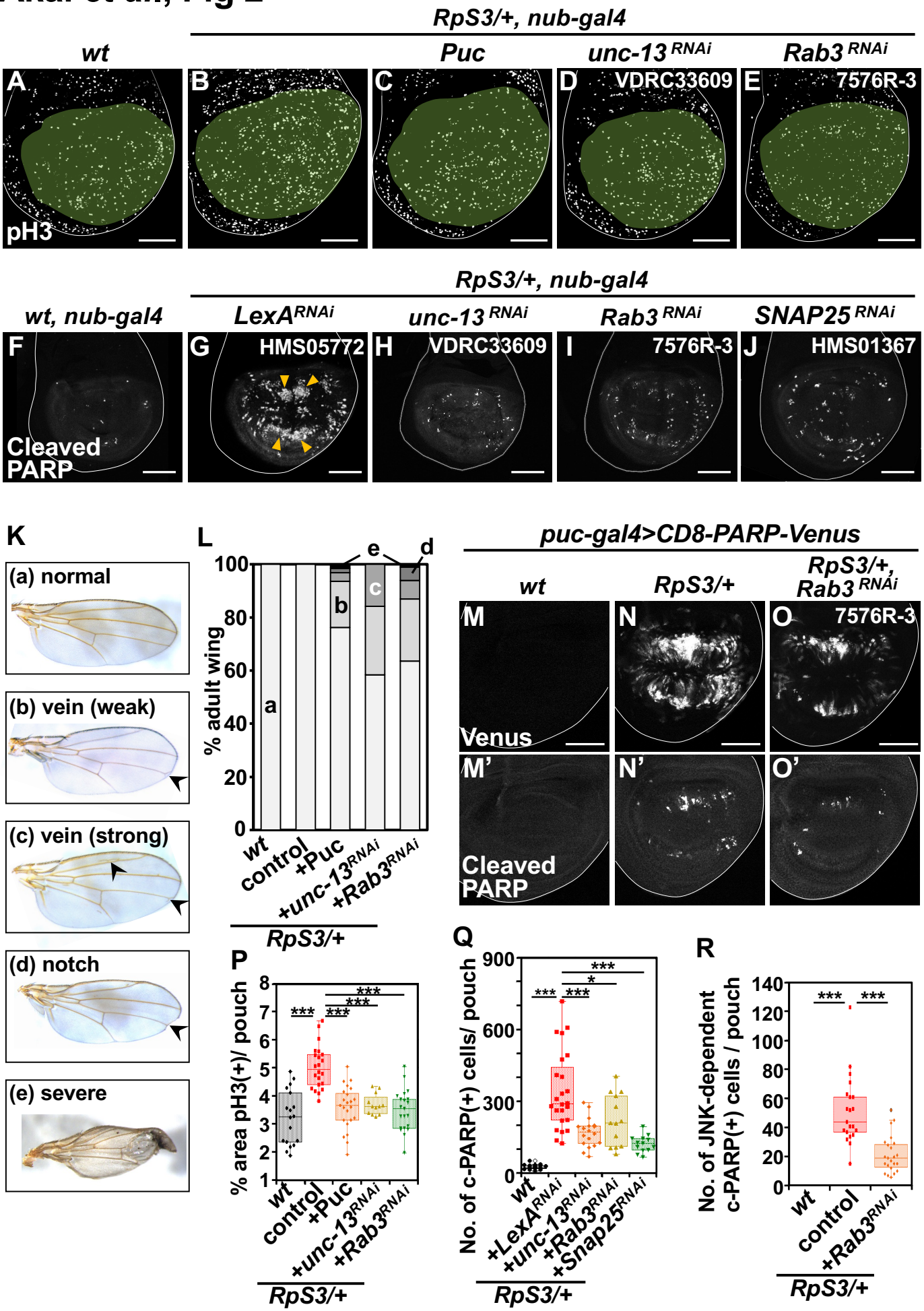

Akai *et al.*, Fig 3

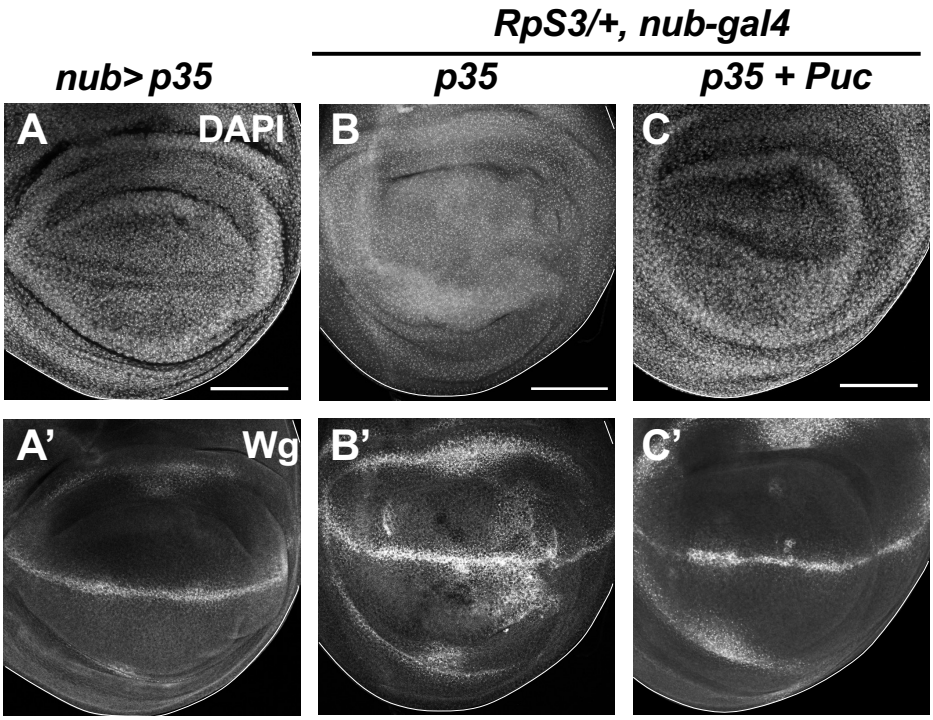

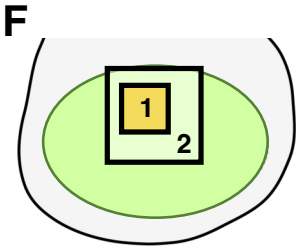

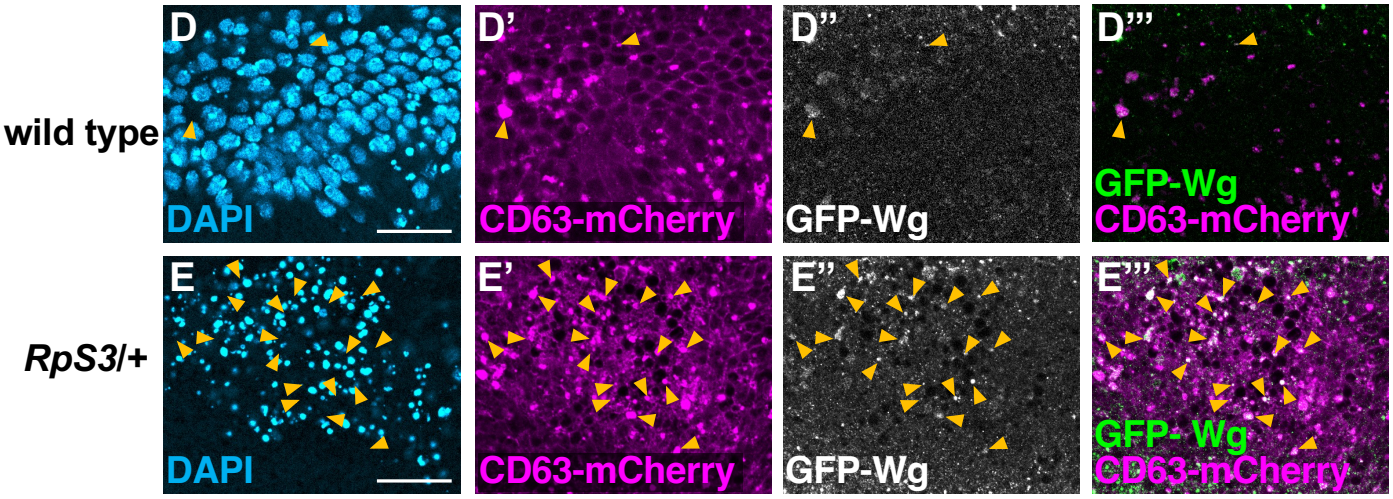

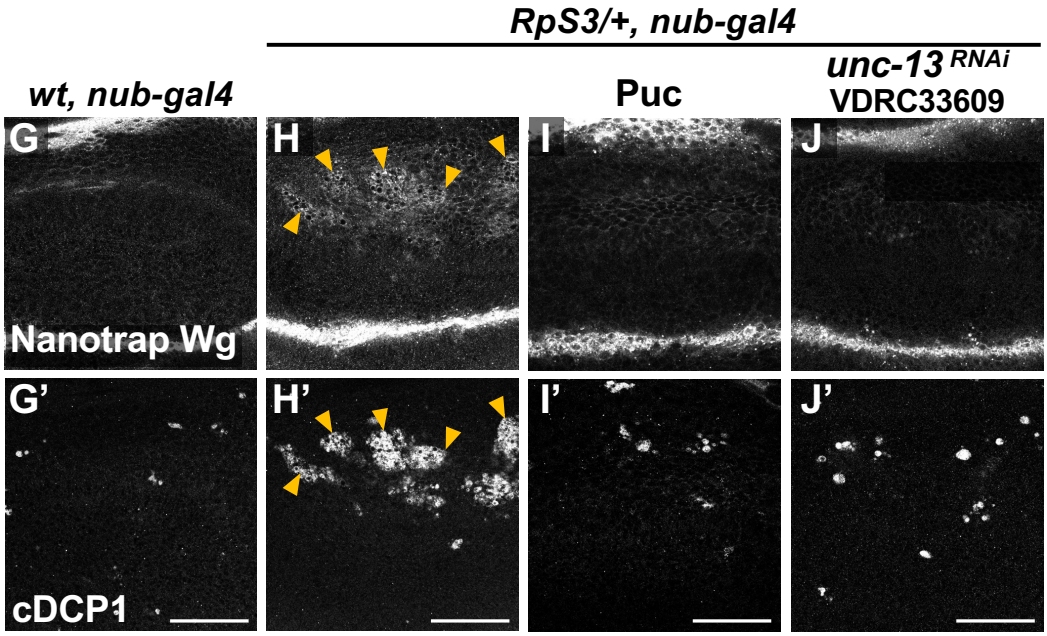

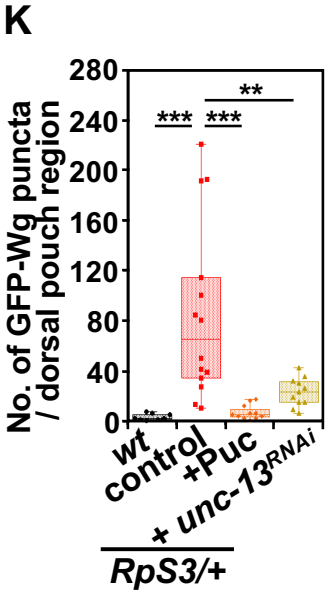

Akai *et al.*, Fig 4

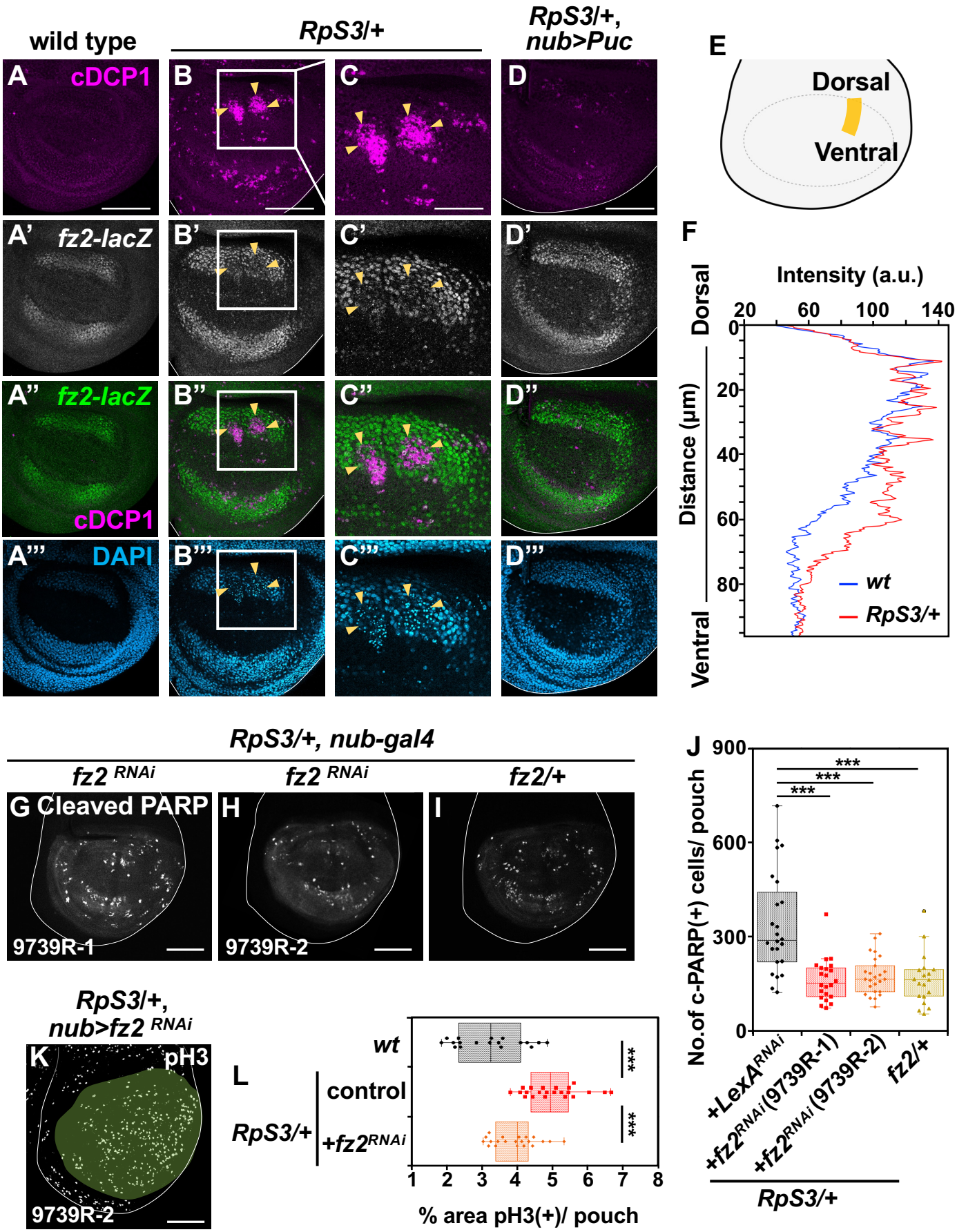

Akai *et al*., Fig 5

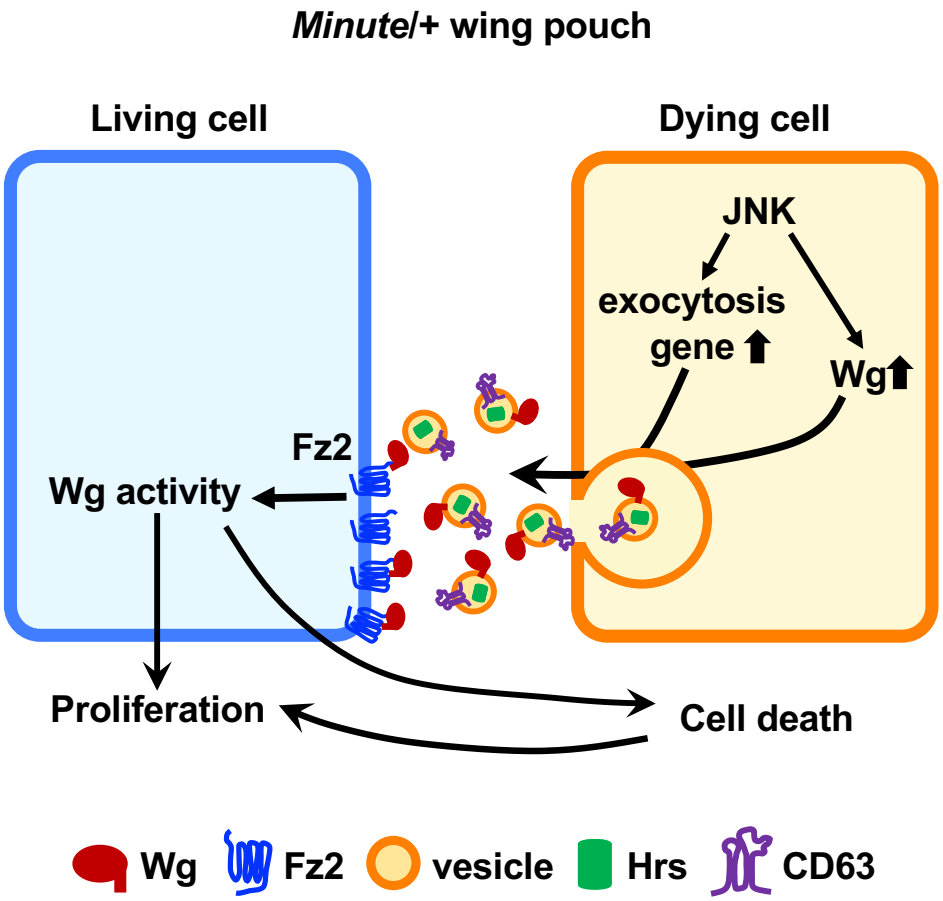

Akai *et al.*, S1

A

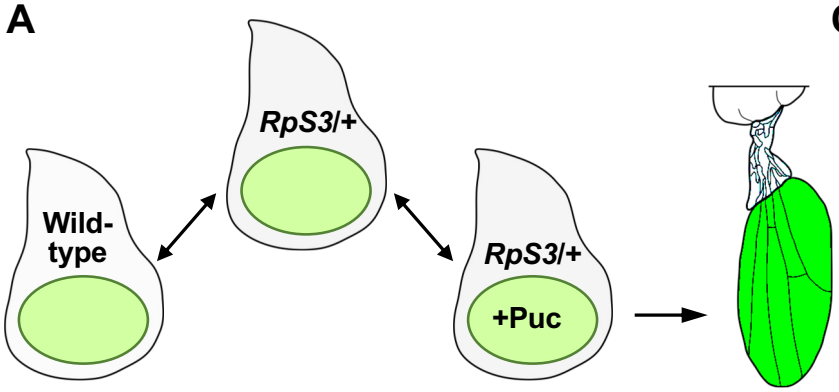

C 1097 *RpS3*/+-regulated genes

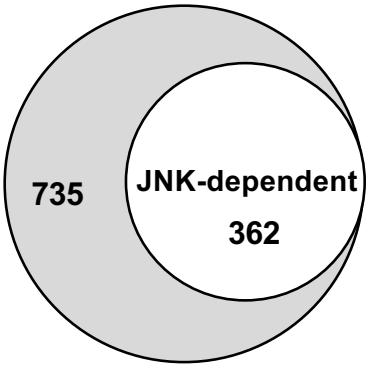

B

GO term	P value
receptor signaling pathway via JAK-STAT	3.82E-04
DNA repair	5.66E-08
positive regulation of JNK cascade	2.25E-04
secretion by cell	1.06E-03

D

	Fold change	secretion by cell	
gene	*unc-13*	*SNAP25*	*cadps*
RpS3/+ / Wild-type	5.97	82.14	2.29
RpS3/+ / *RpS3*/+, +Puc	2.42	2.52	3.44

F

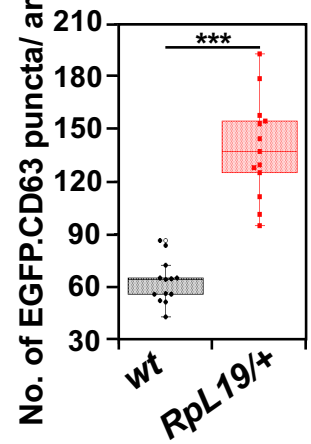

RpL19/+

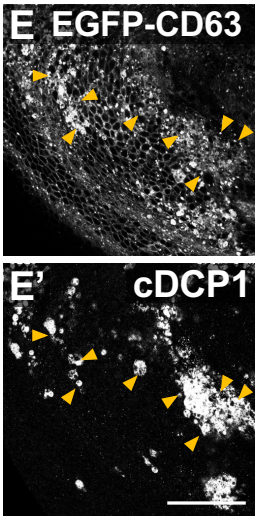

wt *RpS3/+*

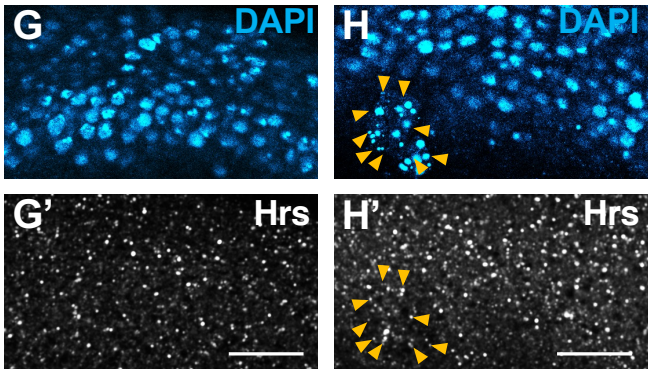

I

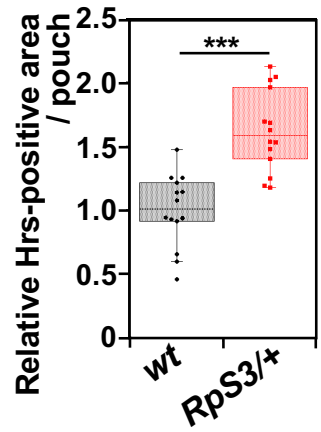

Akai *et al.*, S2

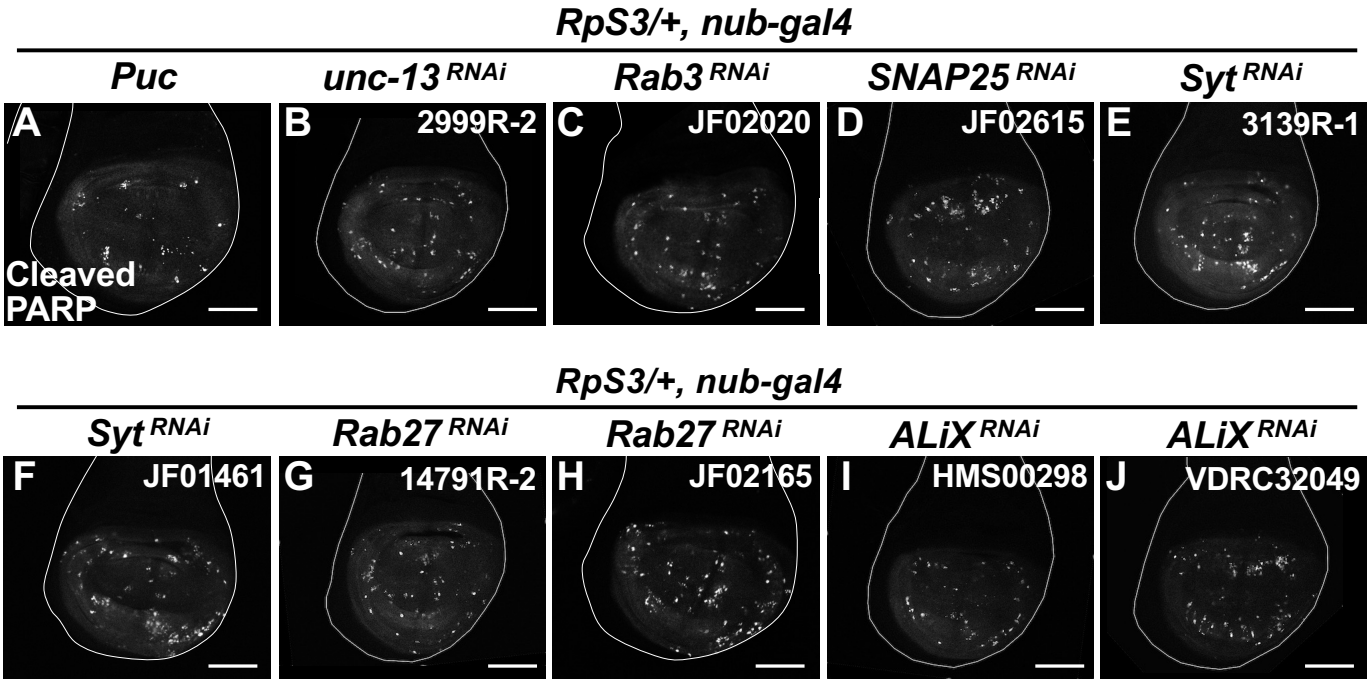
RpS3/+, nub-gal4
Puc
unc-13 RNAi
Rab3 RNAi
SNAP25 RNAi
Syt RNAi
A
Cleaved PARP
B
2999R-2
C
JF02020
D
JF02615
E
3139R-1
RpS3/+, nub-gal4
Syt RNAi
Rab27 RNAi
Rab27 RNAi
ALiX RNAi
ALiX RNAi
F
JF01461
G
14791R-2
H
JF02165
I
HMS00298
J
VDRC32049

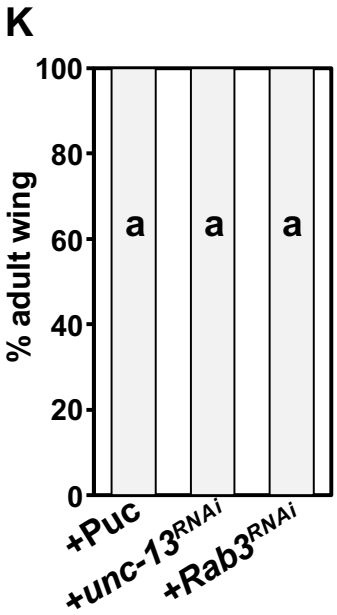
K
% adult wing
100
80
60
40
20
0
a
a
a
+Puc
+unc-13RNAi
+Rab3RNAi

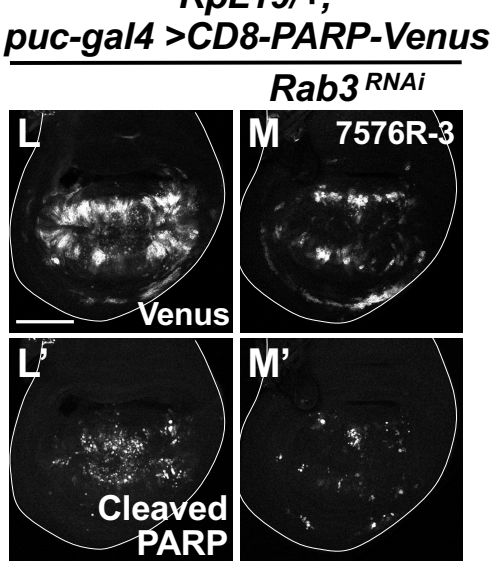
RpL19/+,
puc-gal4 >CD8-PARP-Venus
Rab3 RNAi
L
M
7576R-3
Venus
L'
M'
Cleaved PARP

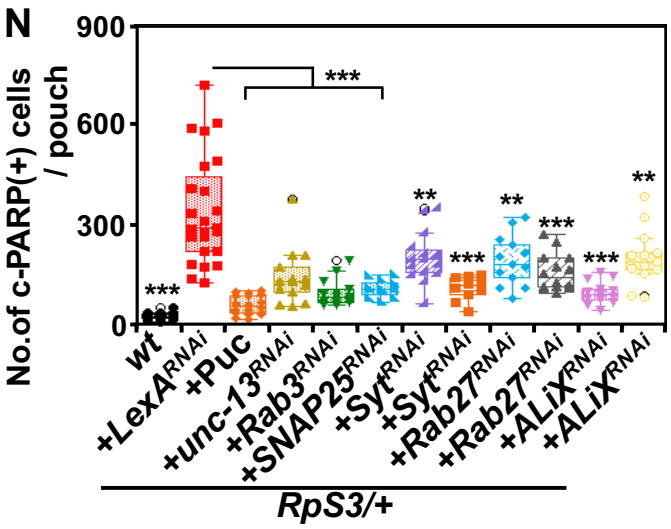
N
No.of c-PARP(+) cells / pouch
900
600
300
0
***
**
wt
+LexARNAi
+Puc
+unc-13RNAi
+Rab3RNAi
+SNAP25RNAi
+SytRNAi
+SytRNAi
+Rab27RNAi
+Rab27RNAi
+ALiXRNAi
+ALiXRNAi
RpS3/+

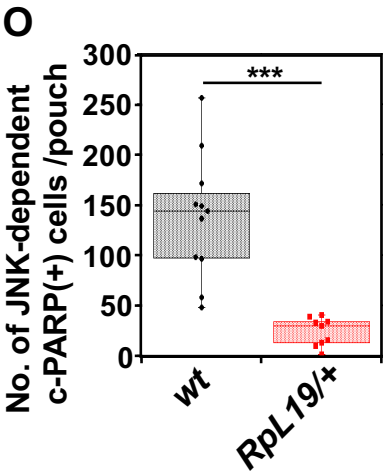
O
No. of JNK-dependent c-PARP(+) cells /pouch
300
250
200
150
100
50
0
***
wt
RpL19/+

Akai *et al.*, S3

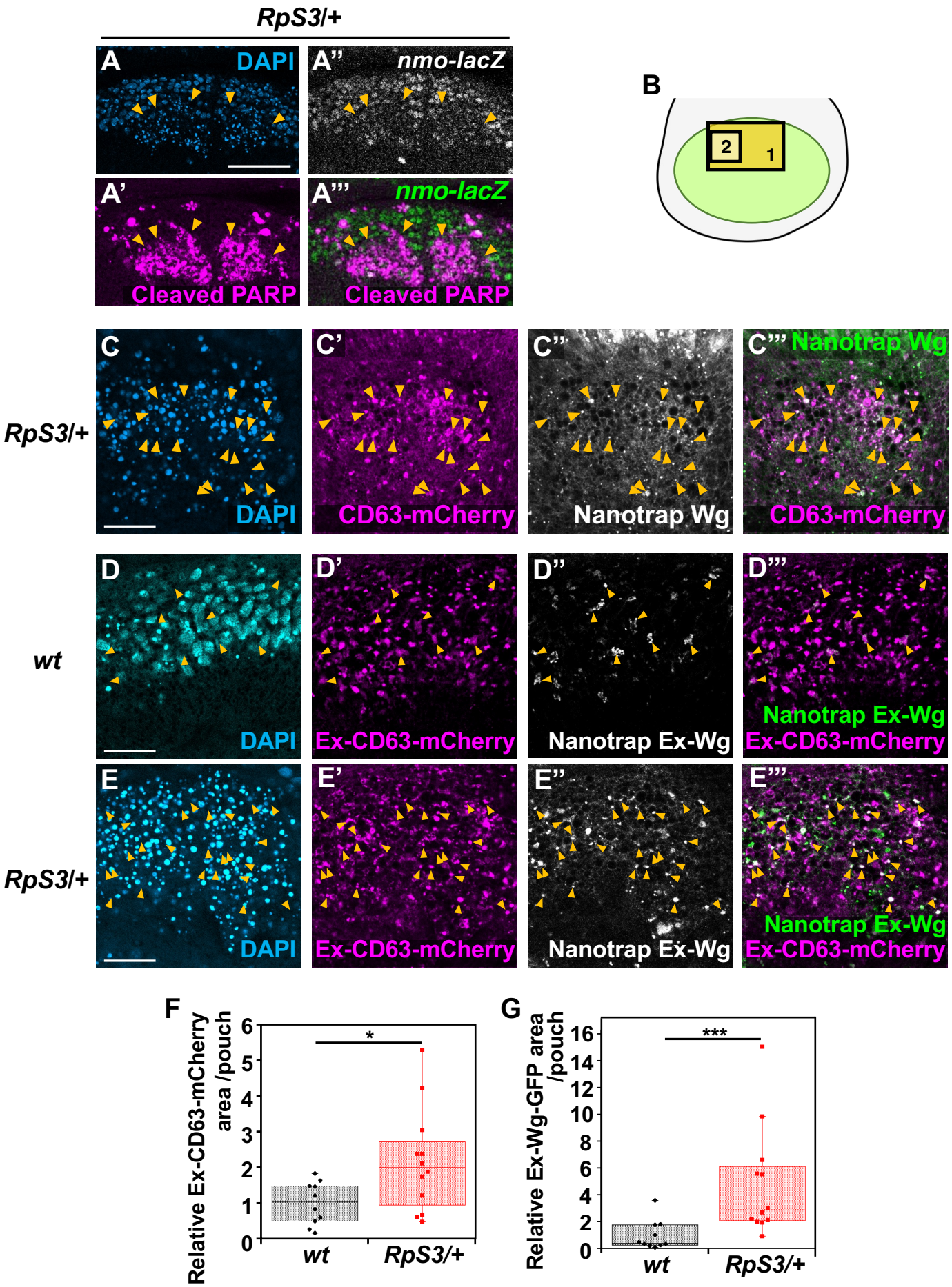
RpS3/+
A
DAPI
A''
nmo-lacZ
A'
Cleaved PARP
A'''
nmo-lacZ
Cleaved PARP
B
2
1
RpS3/+
C
DAPI
C'
CD63-mCherry
C''
Nanotrap Wg
C'''
Nanotrap Wg
CD63-mCherry
wt
D
DAPI
D'
Ex-CD63-mCherry
D''
Nanotrap Ex-Wg
D'''
Nanotrap Ex-Wg
Ex-CD63-mCherry
RpS3/+
E
DAPI
E'
Ex-CD63-mCherry
E''
Nanotrap Ex-Wg
E'''
Nanotrap Ex-Wg
Ex-CD63-mCherry
F
Relative Ex-CD63-mCherry area /pouch
0
1
2
3
4
5
6
*
wt
RpS3/+
G
Relative Ex-Wg-GFP area /pouch
0
2
4
6
8
10
12
14
16
***
wt
RpS3/+

Akai *et al*., S4

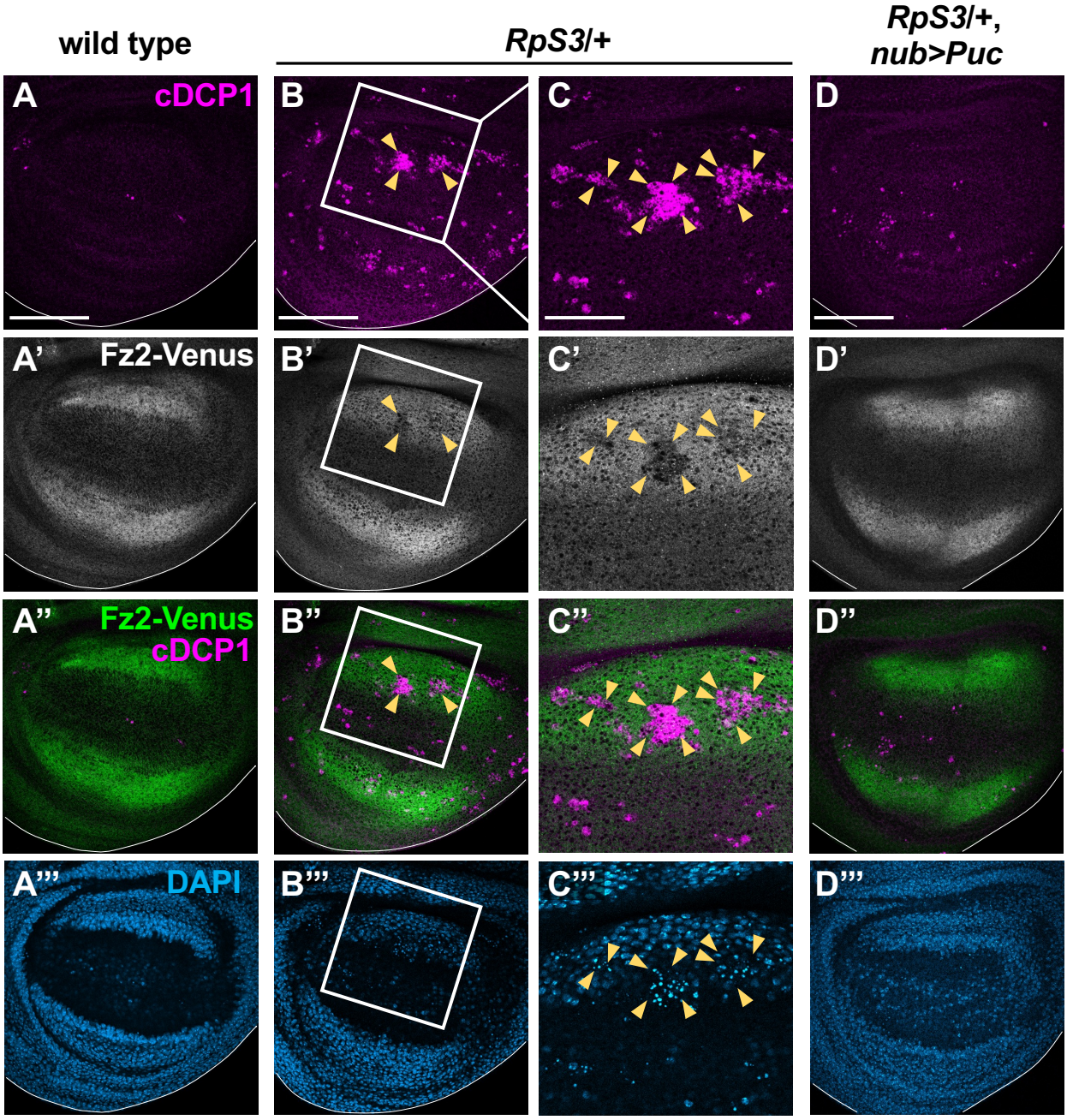
wild type
RpS3/+
RpS3/+, nub>Puc
A
cDCP1
B
C
D
A'
Fz2-Venus
B'
C'
D'
A''
Fz2-Venus
cDCP1
B''
C''
D''
A'''
DAPI
B'''
C'''
D'''